Giant spontaneous polarization for enhanced ferroelectric property of biaxially oriented poly(vinylidene fluoride) by mobile oriented amorphous fractions †

Guanchun Rui,[1,#] Yanfei Huang,[2,#] Xinyue Chen,[1] Ruipeng Li,[3] Dingrui Wang,[4] Toshikazu Miyoshi,[4] Lei Zhu[1,*]

[1] *Department of Macromolecular Science and Engineering, Case Western Reserve University, Cleveland, Ohio 44106-7202, United States*

[2] *College of Materials Science and Engineering, Shenzhen Key Laboratory of Polymer Science and Technology, Shenzhen University, Shenzhen 518055, P. R. China*

[3] *National Synchrotron Light Source II, Brookhaven National Laboratory, Upton, New York 11973, United States*

[4] *Department of Polymer Science, University of Akron, Akron, Ohio 44325-3909, United States*

† Electronic supplementary information (ESI) available. See DOI: 10.1039/x0xx00000x

# These authors contribute equally to this work.

* Corresponding author. Email: lxz121@case.edu (L. Zhu)

Abstract

Poly(vinylidene fluoride) (PVDF) and its random copolymers exhibit the most distinctive ferroelectric property; however, their spontaneous polarization (60-105 mC/m^2) is still inferior to those (>200 mC/m^2) of the ceramic counterparts. In this work, we report an unprecedented spontaneous polarization (P_s = 140 mC/m^2) for a highly poled biaxially oriented PVDF (BOPVDF) film, which contains a pure β crystalline phase. Given the crystallinity of ~0.52, the P_s for the β phase ($P_{s,\beta}$) is calculated to be 279 mC/m^2, if a simple two-phase model of semicrystalline polymers is assumed. This high $P_{s,\beta}$ is invalid, because the theoretical limit of $P_{s,\beta}$ is 185 mC/m^2, as calculated by the density functional theory. To explain such a high P_s for the poled BOPVDF, a third component in the amorphous phase must participate in the ferroelectric switching to contribute to the P_s. Namely, an oriented amorphous fraction (OAF) links between the lamellar crystal and the mobile amorphous fraction. From the hysteresis loop study, the OAF content was determined to be ~0.28, more than 50% of the amorphous phase. Because of the high polarizability of the OAFs, the dielectric constant of the poled BOPVDF reached nearly twice the value of conventional PVDF. The fundamental knowledge obtained from this study will provide a solid foundation for the future development of PVDF-based high performance electroactive polymers for wearable electronics and soft robotic applications.

Introduction

High spontaneous polarization (P_s) ferroelectric polymers are functional materials, which find a broad range of applications in piezoelectric, pyroelectric, and electrocaloric cooling devices.[1, 2] Among all ferroelectric polymers, whether amorphous or semicrystalline, poly(vinylidene fluoride) (PVDF) and its random copolymers exhibit the most well-defined ferroelectricity with a high P_s in the range of 50-105 mC/m^2.[3-7] The theoretical limit for the P_s of the β phase ($P_{s,\beta}$) was first calculated to be 130 mC/m^2, corresponding to a dipole moment of 2.1 Debye (or D) for each repeat unit, based on the rigid-dipole model and molecular dynamics simulation.[8-13] However, this value could not explain the experimental P_s of 105 mC/m^2 for PVDF with a crystallinity (x_c) of 0.5-0.6.[4-7] Namely, the maximum $P_{s,\beta}$ could reach as high as 200 mC/m^2, if a simple two-phase model (i.e., crystalline and amorphous phases) is assumed for semicrystalline polymers. Later, using density functional theory (DFT) and taking into account of the strong rigid dipole-electron cloud interaction (note, the molecular dynamics method cannot directly simulate electrons),[14-16] the maximum $P_{s,\beta}$ was calculated to be 185 mC/m^2, about a 50% increase from the rigid dipole model. This actually corresponds to a dipole moment of 3.0 D for each repeat unit. Nonetheless, the maximum $P_{s,\beta}$ of 200 mC/m^2 based on the two-phase model is still higher than this theoretical limit. This observation makes us to speculate that the two-phase model for semicrystalline PVDF is wrong. Actually, the microstructure of semicrystalline PVDF must be more complicated than the simple two-phase model.

It is well-known that chain-folding is a general phenomenon for semicrystalline polymers when crystallized from a dilute solution.[17, 18] It is attributed to the kinetics effect that extended-chain crystals (ECCs) are difficult to form, given the long chain nature of polymers. However, the crystalline morphology of polymers is much complicated when crystallized from the melt[19-21]

or under certain processing conditions, including injection molding,[22] film extrusion,[23] and fiber spinning.[24] The simple two-phase model cannot adequately describe the complicated morphology of semicrystalline polymers and subsequent mechanical, barrier, optical, and electrical performance. Instead, an intermediate fraction exists between the crystalline lamellae and the isotropic amorphous fraction (IAF).[19-21] This intermediate fraction consists of oriented polymer chains stemming out from the crystal basal planes due to either the difficulty in chain-folding or kinetic reasons (e.g., fast crystallization). From the structure point of view, it should be named as the oriented amorphous fraction (OAF).

With one end tethered to the solid lamellar crystal, these amorphous chains in the OAF have reduced mobility, which gradually tapers off from the crystal basal plane into the IAF.[25] Intriguingly, for most semicrystalline polymers, a significant part of the OAF is rather rigid or glassy, and is thus called the rigid amorphous fraction (RAF).[20, 21] On the other hand, a large portion of the IAF remains mobile, and is thus called the mobile amorphous fraction (MAF). Note, OAF and IAF are defined from the structure point of view, whereas RAF and MAF are defined from the chain mobility point of view, which are often determined by temperature-modulated differential scanning calorimetry (TM-DSC). The glass transition temperature (T_g) of RAFs is higher than that of MAF. As temperature increases, the RAF gradually devitrifies and its content decreases.[26, 27] If the increase of $T_{g,RAF}$ is moderate, a broad and increased overall T_g is observed for the entire amorphous phase (i.e., RAF+MAF). Typical examples are poly(ethylene terephthalate) (PET),[26-29] poly(trimethylene terephthalate) (PTT),[30] poly(ethylene naphthalate) (PEN),[31-33] poly(ether ether ketone) (PEEK),[34, 35] isotactic polystyrene (iPS),[36] poly(phenylene sulfide),[37-39] polycarbonate,[40] aliphatic polyamides (PA, e.g., PA6),[41, 42] poly(L-lactide),[43, 44] poly(3-hydroxy-butyrate),[40, 45] and poly(ε-caprolactone).[46] In some cases, the $T_{g,RAF}$

can increase to such a degree that it completely separates from the $T_{g,MAF}$. For instance, isotactic polypropylene (iPP) shows a second $T_{g,RAF}$ around 50 °C in addition to its regular T_g around -5 °C.[47-49] Similarly, isotactic polybutane-1 (iPBu) also exhibits RAF, which devitrifies between 0 and 50 °C ($T_{g,MAF}$ = -25 °C).[47, 50] Given the behavior of iPP and iPBu, polyethylene (PE) should also belong to this category.[51, 52] However, the $T_{g,RAF}$ often becomes too broad to be clearly detected. Poly(butylene terephthalate) (PBT) has a true $T_{g,MAF}$ at -25 °C. After cold crystallization, a second T_g for RAF is observed at 47 °C.[53, 54] PTFE exhibits a second $T_{g,RAF}$ at a temperature (115 °C) much higher than the $T_{g,MAF}$ at -100 °C.[55, 56] In an extreme case, the $T_{g,RAF}$ becomes so high that it is even above the melting temperature (T_m) of the poor crystals. For example, the $T_{g,RAF}$ of poly(2,6-dimethyl-1,4-phenylene oxide) (PPO) is higher than its T_m, when crystallized from the melt with the aid of a plasticizer or a solvent.[57, 58] From these studies, it seems that the polymer chain rigidity is an important factor for how much the $T_{g,RAF}$ separates from the $T_{g,MAF}$. If the polymer chains are already rigid, the difference between $T_{g,RAF}$ and $T_{g,MAF}$ is not large. Therefore, only one broad but increased T_g is observed for MAF+RAF. This is the case for aromatic ring-containing polymers and polymers with strong intermolecular interactions (e.g., aliphatic polyamides and polyesters, polycarbonates). If the polymer chains are quite flexible, the formation of RAF significantly changes the $T_{g,RAF}$; therefore, a separate T_g is observed at higher temperatures. This is the situation for PE, iPP, iPBu, PBT, and PTFE. If the chains are extremely rigid such as in PPO, $T_{g,RAF}$ can increase beyond T_m when the crystals are poor.

Intriguingly, a few dipolar polymers are exceptions and do not exhibit any obvious RAF, as studied by quasi-isothermal TM-DSC.[20] They include poly(ethylene oxide) (PEO),[20] poly(*p*-dioxanone),[59] and aliphatic polyketones.[60] However, given the nature of oriented chains stemming out from the crystal basal planes after melt-crystallization and/or large-scale plastic

deformation, these polymers should contain OAF, even though RAF is not observable by TM-DSC. In this sense, the mobile OAF structure can be considered as more or less a mobile liquid crystal, whereas the RAF structure should be considered as a glassy liquid crystal.

From the literature, a unique family of polar fluoropolymers, including PVDF and its random copolymers, has not been extensively investigated. For example, do they contain any OAF? If yes, is the OAF rigid (i.e., RAF)? Also, what are the physical effects of the OAF on dielectric and ferroelectric properties? First, for PVDF/poly(methyl methacrylate) (PMMA) blends,[61-65] two T_gs were observed. One is around -35 °C and does not change with the addition of PMMA. The other is found at higher temperatures and varies with the PMMA content. The latter can be attributed to the miscible PVDF/PMMA blends in the amorphous phase. The former is attributed to the OAF at the crystal-amorphous interfaces. Due to its dense packing, no PMMA chains can penetrate into the OAF and change its T_g. Later, we carried out a preliminary broadband dielectric spectroscopy (BDS) study on a biaxially oriented PVDF (BOPVDF) film, which contained 70% α phase and 30% β phase.[66] Through a theoretical estimation using the Debye equation,[66, 67] an OAF was also proposed to explain the high dielectric constant of the amorphous phase in the BOPVDF film. However, no direct evidence was provided in these reports.

Through an ultrafast DSC study,[68] a smaller heat capacity change (0.14 $J \cdot g^{-1}K^{-1}$) was observed at the glass transition than the theoretical value (0.331 $J \cdot g^{-1}K^{-1}$). It was considered to be caused by the RAF in PVDF. By estimating the x_c of the α phase (0.25, weight fraction), the RAF content was calculated to be 0.35. More recently, using TM-DSC, the RAF content was determined to be 0.21-0.28 for the neat α phase PVDF and 0.42-0.46 for the neat β phase PVDF.[69] However, the values of the RAF content were largely influenced by the accuracy of crystallinity

(e.g., the heat of fusion for the perfect β crystal was somewhat overestimated[70]).

Given the ambiguity for the OAF/RAF issue in PVDF-based polymers, we carried out a systematic investigation in this work. A BOPVDF film was extensively polarized unidirectionally above 600 MV/m to convert all α crystals into β crystals. Intriguingly, an unprecedented P_s of 140 mC/m^2 was obtained from the electric displacement (D)-electric field (E) loop measurements. Given the x_c of ~0.52 for this sample, the $P_{s,\beta}$ could reach 279 mC/m^2 if calculated using the two-phase model. Apparently, this is wrong when considering the theoretical limit of $P_{s,\beta}$ = 185 mC/m^2. Therefore, the OAFs are present in the highly poled BOPVDF film and must participate in the ferroelectric switching together with the β crystals to enhance the P_s.

Experimental section

Materials

The fresh BOPVDF film was provided by Kureha Corporation (Tokyo, Japan) with a uniform thickness of 8.0±0.1 μm. Based on our previous report,[66] the crystallinity (x_c) was ca. 0.54 and the crystalline phase contained 70% α and 30% β crystals. The biaxial processing conditions was unknown; however, these could be inferred from the α/β ratio and two-dimensional (2D) wide-angle X-ray diffraction (WAXD) result in ref. 66. Judging from the α/β ratio (i.e., >2) for the BOPVDF, the stretching temperature should be above 120 °C, as discussed before.[71-73] Since the $(110)_\alpha$ reflection was much stronger in the machine direction (MD) than in the transverse direction (TD), the film must be stretched sequentially by a tenter-line processing and the stretching ratio was higher in the MD.[23] The BOPVDF film was thoroughly dried in vacuum at 50 °C for 3 days and stored in a desiccator before use.

Gold (Au) electrodes (10-15 nm) were coated on both sides of the film with the electrode

area being either 7.06 or 78.5 mm^2, using a Q300TD sputter coater (Quorum Technologies, Ltd., U.K.). High-field unidirectional electric poling was applied at room temperature to transform all the α crystals into the β crystals, using the Premiere II ferroelectric tester (Radiant Technologies, Inc., Albuquerque, NM) in combination with a Trek 10/10B-HS high-voltage amplifier (0-10 kV AC, Lockport, NY). The poling field was 600-650 MV/m with a unidirectional (i.e., rectified) sinusoidal waveform at 10 Hz, and the sample was repeatedly polarized for at least 80 times at 600 MV/m or 40 times at 650 MV/m. It was reported that unidirectional poling was more beneficial than bipolar poling to reach high dielectric breakdown strengths for polymer films.[74]

PVDF pellets were purchased from Sigma-Aldrich (St. Luis, MO), and the vendor reported weight-average molecular weight (M_w) was 534,000 g/mol. Using hot-compression, melt-recrystallized (MR) PVDF films with thickness around 30-40 μm were obtained. P(VDF-*co*-hexafluoropropylene) [P(VDF-HFP)] resin was also purchased from Sigma-Aldrich, which contained 4 mol.% HFP comonomer. The vendor reported a M_w of 400000 g/mol with a dispersity of 3.1. The P(VDF-HFP) film was obtained by solution-casting (SC) from a 4 wt.% solution in tetrahydrofuran (THF) onto a silicon wafer at room temperature.[75] The SC P(VDF-HFP) film thickness was ca. 15 μm.

Characterization and instrumentation

A solid-state proton nuclear magnetic resonance (^{1}H ssNMR) echo (90-τ-90-τ) experiment was conducted using a Bruker AVANCE III 300 MHz instrument equipped with a 4 mm double resonance probe. The ^{1}H resonance frequency is 300.1 MHz. The ^{1}H 90° pulse was 2.3 μs and the echo delay time (τ) was set to 7 μs to record all of the proton signals. Peaks were fitted with Gaussian and Lorentzian functions using the Igor software.

Attenuated total reflection (ATR) mode FTIR experiments were performed using an Agilent Cary 630 FTIR spectrometer (Agilent Technologies, Santa Clara, CA), using diamond as the ATR crystal. The data was collected with 32-scans and the resolution was 4 cm^{-1}. DSC experiments were carried out on a TA Discovery DSC 250. Approximately 3 mg samples were used at a scanning rate of 10 °C/min.

Small-angle X-ray scattering (SAXS) and wide-angle X-ray diffraction (WAXD) experiments for the BOPVDF films were performed at the 11-BM Complex Materials Scattering (CMS) beamline at the National Synchrotron Light Source II (NSLS-II), Brookhaven National Laboratory (BNL). The X-ray wavelength (λ) was 0.0918 nm. An in-vacuum Pilatus 800 K detector (Dectris, Baden-Dättwil, Switzerland) was used for WAXD data collection. A Pilatus 2M detector was used for 2D SAXS experiments. The distances between the sample and the WAXD and SAXS detectors were 373 and 3000 mm, respectively, as calibrated by silver behenate with the first-order reflection at a scattering vector of q = 1.076 nm^{-1}, where $q = (4\pi \sin\theta)/\lambda$ with θ being the half-scattering angle. Typical data collection time was 10 s. One-dimensional (1D) WAXD and SAXS curves were obtained by integration of the corresponding two-dimensional (2D) WAXD and SAXS patterns, respectively.

BDS measurements were carried out on a Novocontrol Concept 80 dielectric spectrometer with temperature control (Novocontrol Technologies GmbH & Co., Montabaur, Germany). The frequency ranged from 1 to 10^7 Hz and the temperature ranged from -100 to 200 °C. The applied voltage was 1.0 V_{rms} (root-mean square voltage). Au electrodes (78.5 mm^2) were sputter coated on both sides of the film for the BDS studies.

D-E loop measurements were performed on the Radiant Premiere II ferroelectric tester. To ensure good contact, Au was sputter-coated on both sides of the film sample as electrodes (7.06

mm^2). The applied voltage had either a bipolar or a unipolar sinusoidal waveform at 10 Hz. The Au-coated film samples were immersed in silicon oil to avoid corona discharge in the air. A home-built sample fixture was used to connect the Au electrodes on both sides of the film sample with the interface of the Radiant ferroelectric tester using high-voltage cables. Temperature was controlled by an Arex-6 Conn. Pro System heating stage (Chemglass, Vineland, NJ).

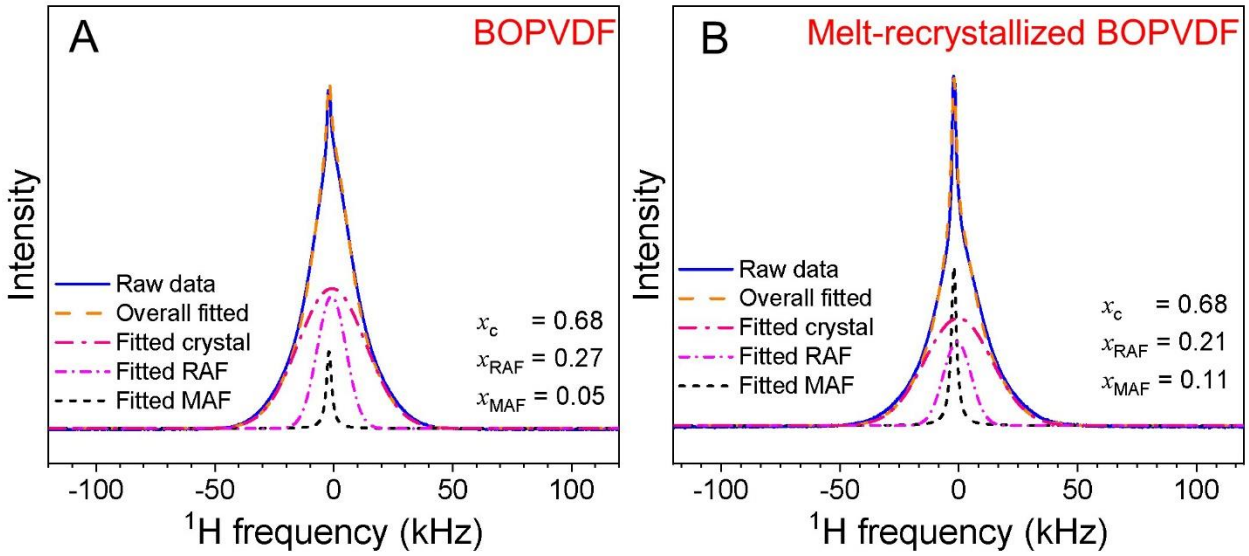

Fig. 1. Baseline-normalized ^{1}H ssNMR at room temperature for (A) BOPVDF and (B) melt-recrystallized BOPVDF. The echo delay time (τ) was set to 7 μs. After peak-fitting (Gaussian functions for the crystals and RAF and Lorentzian function for the MAF), the contents of RAF (x_{RAF}) and MAF (x_{MAF}), and crystallinity (x_c) are shown.

Results and discussion

Direct evidence of the RAF in the BOPVDF film

From our previous study,[66] the OAF was proposed to explain the high dielectric constant for the amorphous phase in the fresh BOPVDF film, which contained 70% α and 30% β phases. However, no direct evidence was provided to support the existence of OAF. Broadline ssNMR technique can be used to provide information about microdomains with different chain mobilities in heterogeneous polymers.[76, 77] In this study, ^{1}H broadline ssNMR was used to demonstrate the

existence of RAF in the BOPVDF film by comparing the fresh and MR samples. The MR sample was obtained by melting at 180 °C followed by natural cooling to room temperature. Note that ssNMR detects polymer chain mobility; therefore, we will use RAF, rather than OAF, for the discussion. The baseline-normalized ^{1}H NMR spectra for the fresh and the MR samples are shown in Fig. 1. Both spectra could not be well-fitted using a simple two-phase model. Instead, a reasonable fitting could be obtained by using a three-phase model, i.e., a broad Gaussian peak for the most immobile domain (i.e., crystals), an intermediate Gaussian peak for the RAF, and a sharp Lorentzian peak for the MAF. Using peak-fitting, the least mobile component (e.g., the crystalline phases) was around 0.68. For the fresh BOPVDF sample, $x_{RAF} = 0.27$ and $x_{MAF} = 0.05$ (Fig. 1A). For the MR sample, $x_{RAF} = 0.21$ and $x_{MAF} = 0.11$ (Fig. 1B). Therefore, the fresh BOPVDF sample contained more RAF than the MR sample. This is understandable because biaxial orientation during the tenterline processing must have resulted in a higher RAF content, and the lamellar crystals from melt-recrystallization should have adopted more chain-folding rather than RAF. Although ssNMR provided direct evidence of the RAF in the BOPVDF film, it could not accurately determine the content of three components (i.e., crystal, RAF, and MAF), because the peak shape also depended on the echo delay time. As reported before for biaxially oriented PET,[78] the rigid component (i.e., short ^{1}H spin-spin relaxation time component) significantly decayed with increasing the echo delay time. Therefore, we could not ignore the echo delay time effect on the rigid components, and we had to resort to other experimental methods to accurately quantify the RAF content.

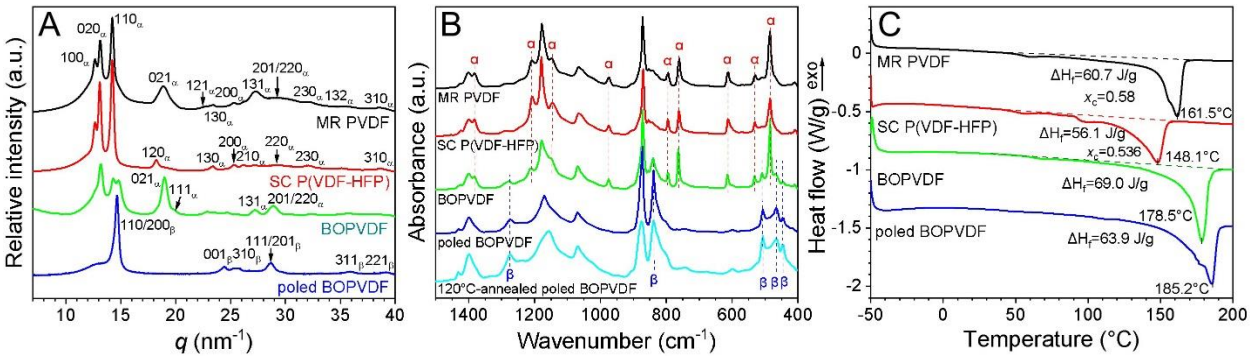

Fig. 2. (A) 1D XRD profiles, (B) FTIR spectra, and (C) DSC first heating curves for the fresh BOPVDF, the highly poled BOPVDF, the MR PVDF, and SC P(VDF-HFP) films. In (B), the FTIR spectrum for the 120 °C-annealed poled BOPVDF film is also included.

Structural characterization for various PVDF and P(VDF-HFP) samples

To determine the x_{OAF}, various PVDF and P(VDF-HFP) samples were prepared. Especially, the BOPVDF was unidirectionally poled (10 Hz with a rectified sinusoidal waveform) at 600 MV/m for 80 times or 650 MV/m for 40 times to convert all α crystals into β crystals. Note that unidirectional poling at only 500 MV/m for 100 times would not fully convert all α crystals into β crystals (ca. 20% α phase left); see Fig. S1 in the Supporting Information. As shown in the 1D XRD profiles in Fig. 2A, the highly poled BOPVDF film exhibited pure reflections from the β phase: $(110/200)_\beta$, $(001)_\beta$, $(310)_\beta$, $(111/201)_\beta$, $(311)_\beta$, and $(221)_\beta$. Meanwhile, its FTIR spectrum in Fig. 2B also showed pure β-phase absorption bands: 1275, 838, 508, 465, and 445 cm^{-1}. Obviously, extensive unipolar poling produced a BOPVDF film with pure β crystals. On the basis of our preliminary study,[66] all crystals were oriented with their *c*-axes along the stretching directions. Also, the stretching ratio along the machine direction (MD) was higher than that along the transverse direction (TD), indicating that the biaxial orientation was sequential during the tenterline processing.

In addition, we also include a hot-pressed MR PVDF film (30-40 μm) and an SC P(VDF-HFP) film (15 μm)[75] in this study. From the XRD results in Fig. 2A, both samples exhibited pure

α crystal reflections. In the FTIR spectra in Fig. 2B, only α phase absorption bands were seen. Therefore, the MR PVDF and SC P(VDF-HFP) films only contain the nonpolar α phase crystals. Due to the quiescent crystallization from the melt, the MR PVDF had a random crystal orientation. The SC P(VDF-HFP) film had an in-plane crystal orientation with the *c*-axis parallel to the film normal direction (ND), as reported in our previous publication.[75]

Fig. 2C shows the DSC first heating curves for these samples. For the MR PVDF, the SC P(VDF-HFP), and the fresh BOPVDF, a weak endothermic peak was seen between 50 and 70 °C, which was attributed to the melting of poor secondary crystals as reported before.[66] The T_m and heats of fusion (ΔH_f, integration started from 40 °C to include the melting of secondary crystals) were labeled in Fig. 2C. Assuming the heat of fusion of the α-ECCs ($\Delta H_f°$) of PVDF is 104.6 J/g,[79] the α-phase x_c values for the MR PVDF and SC P(VDF-HFP) were determined to be 0.58 and 0.536, respectively. Because the heat of fusion for the β-ECCs of PVDF has not been accurately determined, the x_c values for the fresh and poled BOPVDF films could not be accurately calculated from the DSC results. Instead, the x_c was estimated using the XRD result for the poled BOPVDF film to be ca. 0.52 (see Fig. S2). This value is similar to the x_c (0.54) determined by DSC for the fresh BOPVDF film, as we reported before.[66]

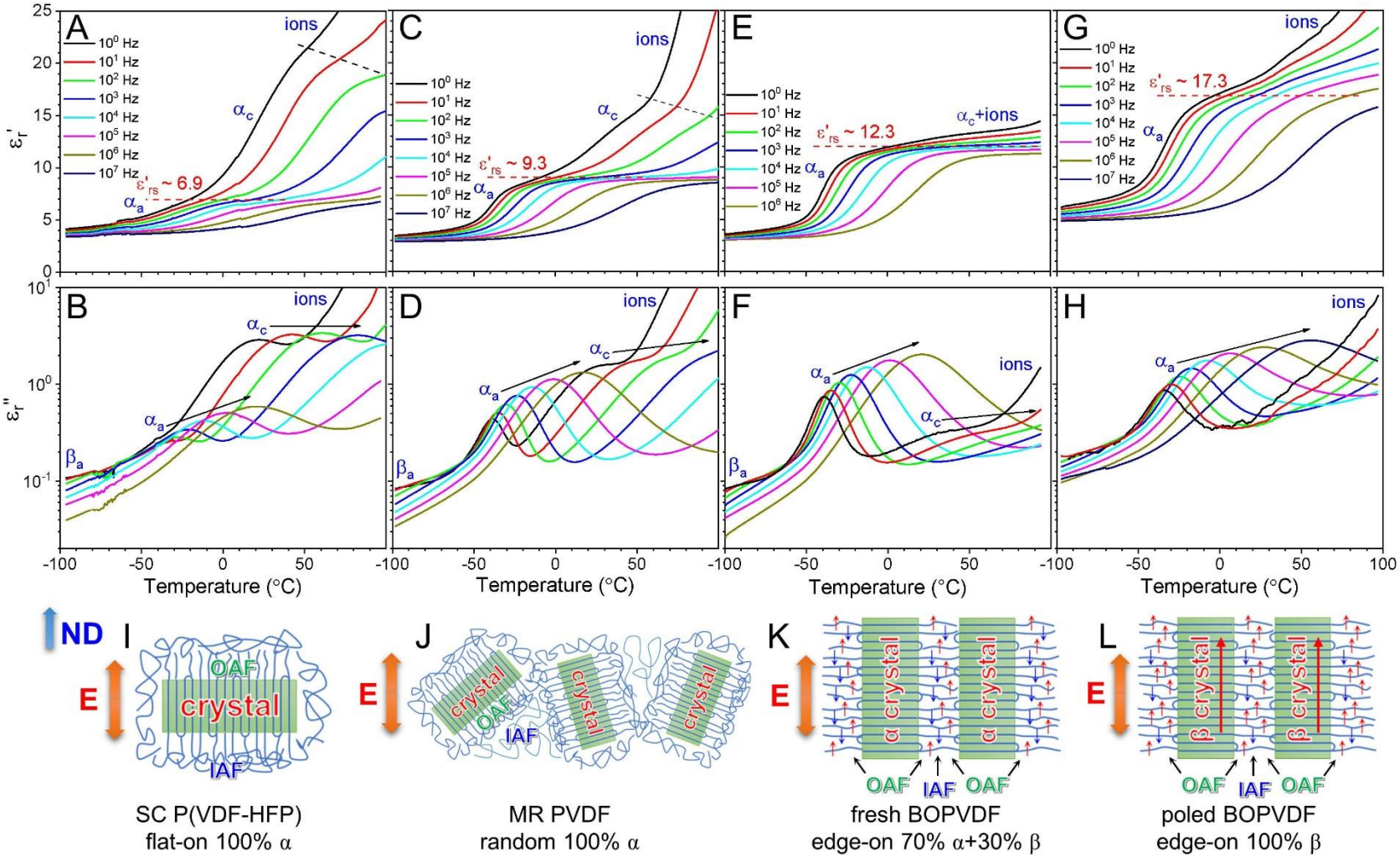

Fig. 3. Temperature-scan BDS results of (A,C,E,G) ε_r' and (B,D,F,H) ε_r'' for various PVDF and P(VDF-HFP) samples. (A,B) Solution-cast (SC) P(VDF-HFP) 96/4 (mol./mol.) from THF with 100% flat-on α crystals (DSC x_c = 0.536).[56] (C,D) Melt-recrystallized (MR) PVDF with randomly oriented 100% α crystal (DSC x_c = 0.58). (E,F) The fresh BOPVDF film with 70% α and 30% β edge-on crystals.[50] (G,H) The poled BOPVDF with 100% edge-on β crystal (XRD x_c = 0.52). The bottom panel shows schematic representation of different crystal orientations with respect to the normal direction (ND) of the film: (I) SC P(VDF-HFP), (J) MR PVDF, (K) fresh BOPVDF, and (L) poled BOPVDF.

Mobile OAF in PVDF-based polymers

Although the RAF content has been estimated for both α and β PVDF samples by DSC studies,[68, 69] questions still remain: Is the OAF in PVDF-based polymers as rigid as a glass around room temperature? If not, what are the effects of the OAF on dielectric and ferroelectric properties of PVDF? To answer these questions, BDS was used to study the mobility of the OAF for various PVDF and P(VDF-HFP) samples. Fig. 3 shows the temperature-scan BDS results of the real (ε_r') and the imaginary (ε_r'') relative permittivities under different frequencies for these polymers. From the BDS results, various dielectric events were observed. Around -80 °C at 1 Hz, the β relaxation for the amorphous phase was observed. It is attributed to localized motion of the frozen PVDF chains.[64, 80] Around -40 °C at 1 Hz, the α_a relaxation for the amorphous phase was observed, and it is due to the micro-Brownian (or cooperative segmental) motion of amorphous PVDF chains. Around 20 °C at 1 Hz, the α_c relaxation of the α crystals was observed, and it is attributed to the wagging motion of tilted CF_2 dipoles along the twisted chains in the α crystal.[66, 81] This relaxation was obvious for the SC P(VDF-HFP) and the MR PVDF, less obvious for the fresh BOPVDF (due to the in-plane crystal orientation), and disappeared for the poled BOPVDF (no α crystals). Above 50 °C, high conduction of impurity ions was observed due to thermally activated detrapping of ions in the PVDF matrix (although the impurity ion level in suspension PVDF samples is only about 0.1 ppm).[82] Upon increasing the frequency, all these transitions shifted to higher temperatures.

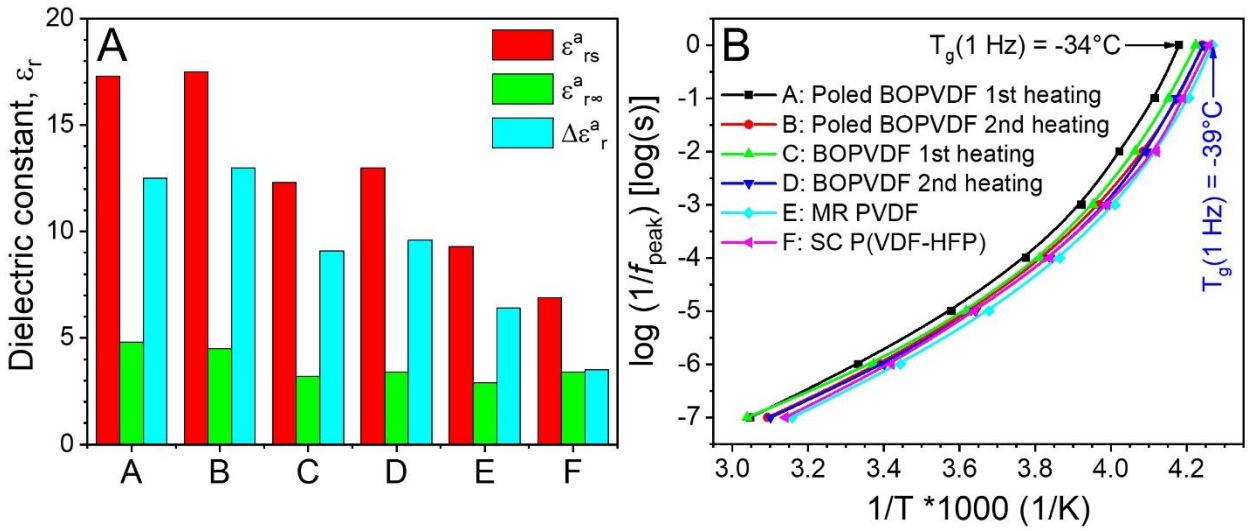

Fig. 4. (A) Summary of dielectric constants, ε^a_{rs}, $\varepsilon^a_{r\infty}$, and dielectric strength ($\Delta\varepsilon^a_r = \varepsilon^a_{rs} - \varepsilon^a_{r\infty}$), for the α_a relaxation in various PVDF polymers (Fig. 3). (B) Log($1/f_{peak}$) as a function of 1/T for these polymers. f_{peak} is the peak frequency of the α_a relaxation in Fig. 3B,D,F,H.

To obtain the contribution of the α_a relaxation to the dielectric constant, we determined the static dielectric constant (ε^a_{rs}) and the high-frequency dielectric constant ($\varepsilon^a_{r\infty}$) for the α_a relaxation. Here, the ε^a_{rs} was taken as the ε_r' value at 20 °C and 1 kHz, and the $\varepsilon^a_{r\infty}$ was taken as the ε_r' value at -100 °C and 10^7 kHz. Note, the contribution from the α_c relaxation in the α crystals should be avoided for the determination of ε^a_{rs}. Then, the dielectric strength ($\Delta\varepsilon^a_r$), defined as $\Delta\varepsilon^a_r = \varepsilon^a_{rs} - \varepsilon^a_{r\infty}$, should reflect the contribution of the α_a relaxation to the dielectric constant. Results of ε^a_{rs}, $\varepsilon^a_{r\infty}$, and $\Delta\varepsilon^a_r$ are summarized in Fig. 4A. Intriguingly, these PVDF samples showed drastically different ε^a_{rs}. At 20 °C and 1 kHz, the SC P(VDF-HFP) film with flat-on α crystals had a low $\varepsilon^a_{rs} = 6.9$. The MR PVDF film with random α crystals had an intermediate $\varepsilon^a_{rs} = 9.3$. The fresh BOPVDF with edge-on 70% α/30% β crystals had a high $\varepsilon^a_{rs} = 12.3$, and finally the highly poled BOPVDF with edge-on β crystals had an even higher $\varepsilon^a_{rs} = 17.3$. Meanwhile, $\Delta\varepsilon^a_r$ exhibited the same trend; namely, $\Delta\varepsilon^a_r = 3.5$ for the SC P(VDF-HFP), 6.4 for the MR PVDF, 9.1 for the fresh BOPVDF, and 12.5 for the poled BOPVDF.

There is a clear orientation effect for the dielectric constants of different PVDF samples.

This orientation effect has already been observed by different researchers,[75, 83, 84] and is attributed to differently oriented crystals, whether α or β form. However, BDS is measured in the linear region with an AC voltage of only 1.0 V_{rms}. Under such a low electric field, no dipolar and ferroelectric switching of PVDF crystals could happen. As such, dielectric constants of α and β PVDF crystals should be lower than 3 with only electronic and atomic polarizations (note, the α_c relaxation should be excluded here)[66, 85, 86] A more plausible explanation for different dielectric constants of these PVDF samples would be the existence of the OAFs with different orientations in these samples. For the SC P(VDF-HFP) film, the OAF oriented parallel to the electric field, and -CH_2CF_2- dipoles along the chains should not contribute to the measured capacitance, but only the IAF contributed (Fig. 3I). As a result, the ε_{rs}^{a} (6.9) and $\Delta\varepsilon_{r}^{a}$ (3.5) were rather low. For MR PVDF, the randomly oriented OAF contributed to the dielectric constant (Fig. 3J), and thus the ε_{rs}^{a} (9.3) and $\Delta\varepsilon_{r}^{a}$ (6.4) increased. With the OAF exclusively oriented perpendicular to the electric field (Fig. 3K), the contribution of -CH_2CF_2- dipoles to the dielectric constant was maximized, i.e., the ε_{rs}^{a} (12.3) and $\Delta\varepsilon_{r}^{a}$ (9.1). Finally, for the highly poled BOPVDF, the ε_{rs}^{a} (17.3) and $\Delta\varepsilon_{r}^{a}$ (12.5) further increased because of the high permanent remanent polarization (P_{r0}, see discussion below) to enhance the internal electric field in the sample (Fig. 3L). This case is similar to the hydrogen-bonded polar nanoregions in liquid water, which increase its dielectric constant.[117-119] In other words, we speculated that the large P_{r0} in the highly poled BOPVDF created polar nanoregions in the OAF and thus enhanced the dielectric constant.

The relaxation time for the α_a relaxation was obtained by $1/f_{peak}$, where f_{peak} was the peak frequency in ε_r'' (Fig. 3B,D,F,H). Fig. 4B shows $\log(1/f_{peak})$ as a function of 1/T for different PVDF polymers. As we can see, the poled BOPVDF had the longest relaxation time during the first heating and the MR PVDF exhibited the shortest relaxation time. However, the dynamic T_g

at 1 Hz was -34 °C for the poled BOPVDF and -39 °C for the MR PVDF. This result suggests that the OAF could become rigid (i.e., RAF) around the T_g; however, it quickly devitrified upon heating above the T_g. Note, devitrification of the RAF above the T_g is also observed in other polymers such as PET;[26, 27] however, complete devitrification usually happens at a much higher temperature. Combining both ssNMR and BDS results, we conclude that the liquid crystal-like OAF at room temperature is rather mobile. At this moment, it is still unclear why the OAF in PVDF-based polymers quickly devitrify when heating above the T_g, although it is speculated to be ascribed to the unique dipolar nature of the PVDF chains in OAF. More research is needed to further understand the underlying mechanism.

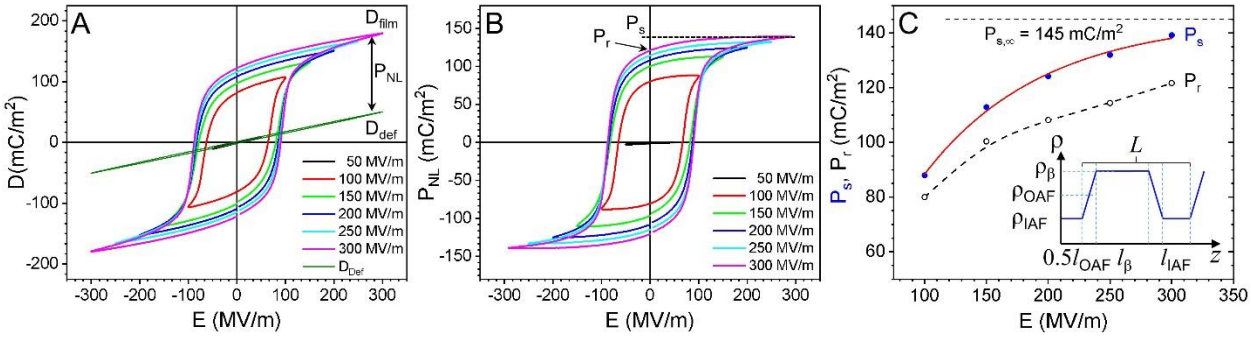

Fig. 5. (A) Bipolar D-E loops for the poled BOPVDF film under different poling electric fields at room temperature. The AC electronic conduction is subtracted for all loops (see Section II in the Supporting Information). In this plot, the linear D-E loop for the deformational polarization (D_{def}) in the sample is also shown.[68] (B) After subtraction of the D_{def} from the film polarization (D_{film}), the nonlinear polarization (P_{NL}) is obtained. From the P_{NL}-E loops, the spontaneous (P_s) and remanent polarization (P_r) are obtained. (C) P_s and P_r as a function of the poling electric field at room temperature. By fitting the P_s data with an exponential decay function, the P_s for the poled BOPVDF film at the infinity electric field ($P_{s,\infty}$) is found to be 145 mC/m^2. The inset shows the hypothesized density profile as a function of distance (z) in the layer normal direction for the β crystal, OAF, and IAF in PVDF.

Determination of x_{OAF} for the poled BOPVDF film

Although both ssNMR and BDS results show the existence of the OAF and its orientation effect on dielectric constants of various PVDF polymers, its quantity is still unknown so far. To

determine the x_{OAF}, D-E loops were measured for the highly poled BOPVDF. Fig. 5A shows the bipolar D-E loops for the highly poled BOPVDF film at room temperature under different poling fields. As shown in Fig. S3, the AC electronic conduction was subtracted for these loops to show pure ferroelectric switching of the β crystals. Meanwhile, the linear D-E loop for the deformational polarization (D_{def}) in PVDF was obtained by a D-E loop study of the polycarbonate (PC)/PVDF multilayer films, as reported before.[87] Here, the deformational polarization in PVDF includes electronic + atomic polarizations of the entire BOPVDF film and the orientational polarization of the amorphous phase. By subtracting the D_{def} loop from the experimental D-E loops, the nonlinear polarization (P_{NL})-E loops were obtained, as shown in Fig. 5B, from which the spontaneous polarization (P_s) and in-situ remanent polarization (P_r) were obtained. Note that the in-situ P_r during the electric poling is different from the permanent P_{r0} after electric poling, because some PVDF dipoles/ferroelectric domains relax after the electric poling.[88] Fig. 5C shows P_s and the in-situ P_r as a function of the poling electric field. By fitting the P_s data with an exponential decay function, the P_s at the infinity electric field ($P_{s,\infty}$) was determined as $P_{s,\infty}$ = 145 mC/m^2 for the poled BOPVDF film. Such a high P_s value has never been reported before. As mentioned above, when the poling field was only 500 MV/m (repeated poling for 100 times), not all the α phase transformed into the β phase, and the P_s at 300 MV/m was significantly lower, only 117 mC/m^2 (see Fig. S1C).

If we consider the crystallinity of 0.52 and only the β crystals contribute to the ferroelectric switching (i.e., the two-phase model), the P_s for the neat β phase ($P_{s,\beta}$) is calculated to be $P_{s,\beta} = P_{s\infty}/0.52$ = 279 mC/m^2. However, as mentioned in the Introduction, DFT calculations predict that the theoretical limit of $P_{s,\beta}$ is 185 mC/m^2.[14-16] Therefore, the calculated value of 279 mC/m^2 using the two-phase model must be incorrect.

We need to use a three-phase model with a finite x_{OAF}, which must also contribute to the nonlinear ferroelectric switching together with the β crystals in the poled BOPVDF film under a high-field electric poling:

$$P_{s,\infty} = x_c P_{s,\beta} + x_{OAF} P_{s,OAF} \quad (1)$$

Here, the x_c and x_{OAF} are molar fractions. Given the same molecular weight for the -CH_2CF_2- repeat units, whether in the crystal or the amorphous phase, the molar fraction should also be the weight fraction. However, it is not the volume fraction, because densities for the β crystal, the OAF, and the IAF are different. When the temperature is above the T_g, the OAF in PVDF polymers is more or less liquid crystalline in nature. Given the gradual transition from the crystal to the IAF (see the density profile in the inset of Fig. 5C), the orientation of chains in the OAF should be tapered, similar to that proposed for the RAF in semicrystalline polymers. Because of the liquid crystalline nature, we consider that ferroelectric domains in the OAF and thus $P_{s,OAF}$ should be induced by the high poling field. After removal of the high poling field, the OAF domains should largely depolarize to exhibit a nearly zero P_{r0}, which is different from the aligned β crystals in the poled BOPVDF film. At this moment, the field-induced $P_{s,OAF}$ is unknown; however, we can do some simple estimation. The maximum x_{OAF} is 1-x_c = 0.48, and thus the minimum $P_{s,OAF}$ is 0.52$P_{s,\beta}$. Then, the maximum $P_{s,OAF}$ is $P_{s,\beta}$, and the minimum x_{OAF} is 0.25.

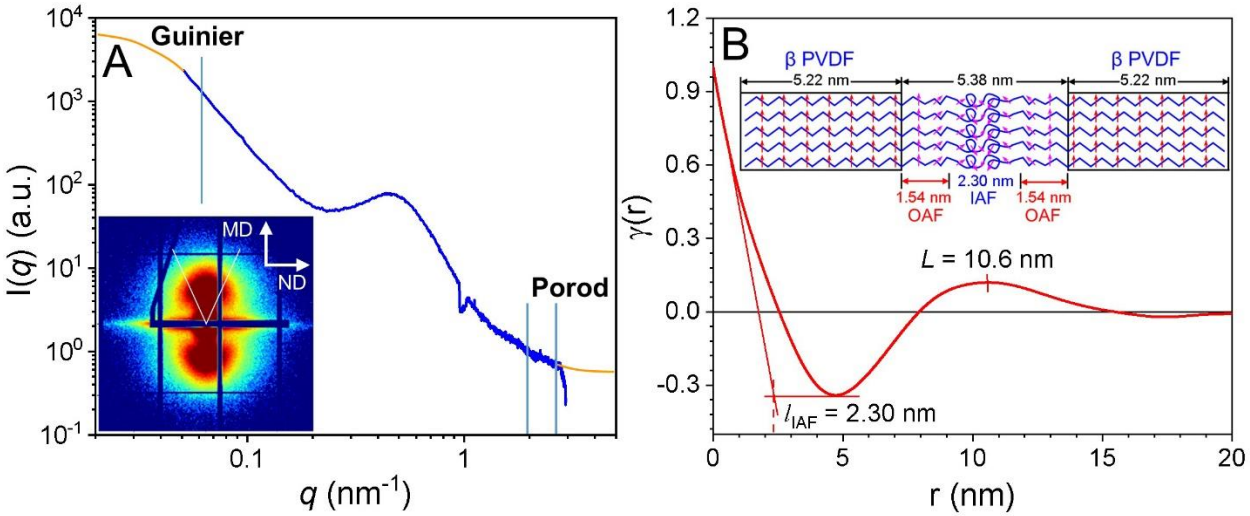

Fig. 6. (A) 1D SAXS profile for the poled BOPVDF film obtained from the integration of the 2D edge-on SAXS pattern in the inset. The X-ray is along the TD with MD in the vertical direction. (B) The correlation function, γ(r), obtained from the SasView software. The inset shows schematic representation of the stacked lamellar structure with the poled β crystals, the OAF, and the IAF. The calculated thicknesses are also indicated.

To more accurately determine the x_{OAF} and $P_{s,OAF}$, we carried out a SAXS analysis for the poled BOPVDF with the correlation function analysis using the SasView software (note, the procedure of SAXS correlation function analysis was described in detail in a previous report[89]). As shown in Fig. 6A, the Guinier function was used for fitting $q \rightarrow 0$ and the Porod model was used for fitting $q \rightarrow \infty$. After subtracting the background and Fourier transformation, the 1D correlation function γ(r) was obtained, as shown in Fig. 6B. From the γ(r), the long period (L) was found at the first maximum: L = 10.6 nm. By extrapolating the linear region of the γ(r) at the low r region to the horizontal minimum line, the average hard-core thickness was found to be ~2.30 nm. Although this extrapolation method should be applied to the two-phase lamellar model, we consider that the OAF behaves more like the β crystal rather than the IAF. Therefore, we attribute this average hard-core thickness to the IAF layer. Given the weight-fraction x_c of 0.52, we have:

$$x_c = \frac{l_\beta \rho_\beta}{l_\beta \rho_{b\beta} + l_{OAF}\rho_{OAF} + l_{IAF}\rho_{IAF}} \quad (2)$$

where l_β and l_{IAF} are layer thicknesses, and ρ_β and ρ_{IAF} are densities of the β crystal (1.972 g/cm^3) and the IAF (1.680 g/cm^3).[66] The l_{OAF} is the OAF layer thickness, and ρ_{OAF} is the average density, $1/2(\rho_\beta + \rho_{IAF})$ = 1.826 g/cm^3. Meanwhile, the long period is:

$$L = l_\beta + l_{OAF} + l_{IAF} \quad (3)$$

Solving Eqns. (2) and (3) by assuming l_{IAF} = 2.30 nm, we obtain l_β = 5.22 nm and l_{OAF} = 3.08 nm. The inset of Fig. 6B shows the schematic representation of the calculated lamellar structure with the IAF sandwiched between two OAF layers (each having a thickness of $0.5l_{OAF}$ = 1.54 nm). Because the β crystals are highly poled in the upward direction, the PVDF chains at the crystal-amorphous interfaces must also have an upward dipole orientation, which gradually relaxes when approaching the IAF. Using these layer thicknesses and densities, weight-fraction x_{OAF} and x_{IAF} can be obtained: x_{OAF} = 0.284 and x_{IAF} = 0.196. Apply this x_{OAF} value in Eqn. (1), we obtain $P_{s,OAF}$ = 166 mC/m^2, which is $0.88P_{s,\beta}$. The smaller $P_{s,OAF}$ than $P_{s,\beta}$ is reasonable, because the OAF is not crystalline but liquid crystal-like. On the basis of the significant x_{OAF} and $P_{s,OAF}$ values, we expect that it is the large amount of mobile OAF and its field-induced polarization that enhances both dielectric and ferroelectric properties for PVDF-based polymers.

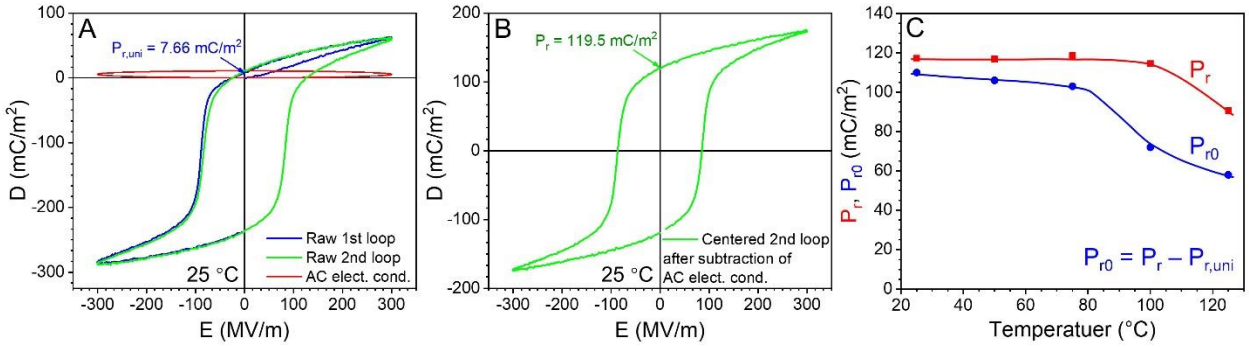

Fig. 7. (A) First two bipolar D-E loops for the poled BOPVDF right after repeated unipolar poling at 600 MV/m for 80 times at 25 °C. The AC electronic conduction is also shown as the

horizontal loop. (B) After subtraction of the AC electronic conduction, the second D-E loop is centered. The poling field is 300 MV/m with a sinusoidal waveform at 10 Hz. (C) In-situ P_r and permanent P_{r0} for the poled BOPVDF as a function of temperatures.

Although the in-situ P_r during bipolar electric poling is shown in Fig. 5C, the permanent P_{r0} is still unknown, which is important for the piezoelectric property.[90, 91] Because of the ferroelectric dipole or domain relaxation,[88] the permanent P_{r0} should be smaller than the in-situ P_r. To determine the permanent P_{r0}, we carried out the following experiment, which is similar to the positive-upward-negative-down (PUND) method.[92] First, the fresh BOPVDF film was extensively polarized unidirectionally at 600 MV/m for 80 times at 25 °C to achieve 100% β crystals. Second, two bipolar loops were recorded while keeping the same poling direction for the first unipolar loop, as shown in Fig. 7A. The remanent polarization for this first unipolar loop was $P_{r,uni}$ = 7.66 mC/m^2. Third, after subtraction of the AC electronic conduction loop from the second bipolar loop followed centering it, the in-situ P_r for the second loop was 119.5 mC/m^2 (Fig. 7B) Therefore, the permanent P_{r0} can be estimated to be at least P_r - $P_{r,uni}$ = 111.8 mC/m^2. Again, this permanent P_{r0} is extremely high compare with the literature values,[3] and we consider that it is this high P_{r0} in the aligned β crystals that induces polar nanoregions for the OAF in the poled BOPVDF and thus a high dielectric constant.

Upon increasing the temperature, the in-situ P_r did not decrease until being annealed at 100 °C for 30 min (Fig. 7C). However, the P_{r0} started to decrease around 80 °C. A similar result was also reported for a commercial uniaxially oriented PVDF film, where the second harmonic generation signal decreased above 80 °C.[93] This is attributed to the decreased ferroelectric domain sizes by thermal motion-induced chain or dipole relaxation in the poled β crystals.

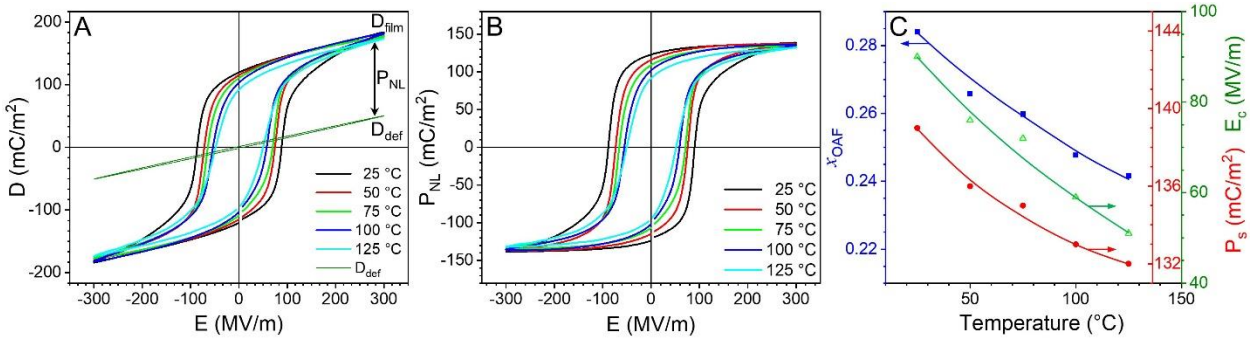

Fig. 8. (A) Bipolar D-E loops for the poled BOPVDF film at different temperatures. The AC electronic conduction is subtracted. Again, the linear D_{def} loop is shown. (B) After subtraction of the D_{def} from the D_{film}, the nonlinear P_{NL}-E loops are obtained at different temperatures. (C) x_{OAF}, P_s, and E_c as a function of the poling electric field at different temperatures. The poling electric field is 300 MV/m with a sinusoidal waveform at 10 Hz.

For the highly poled BOPVDF film, the D-E loop study was also performed at high temperatures (Fig. 8A). After subtraction of the D_{def}, the P_{NL}-E loops are shown in Fig. 8B, from which P_s and E_c values are obtained. As we can see from Fig. 8C, P_s and E_c continuously decreased with increasing temperature, again suggesting the gradual decrease of the domain sizes. By assuming $P_{s,OAF}$ being $0.88P_{s,\beta}$, the x_{OAF} could be calculated at different temperatures; it decreased from 0.284 at room temperature to 0.243 at 125 °C.

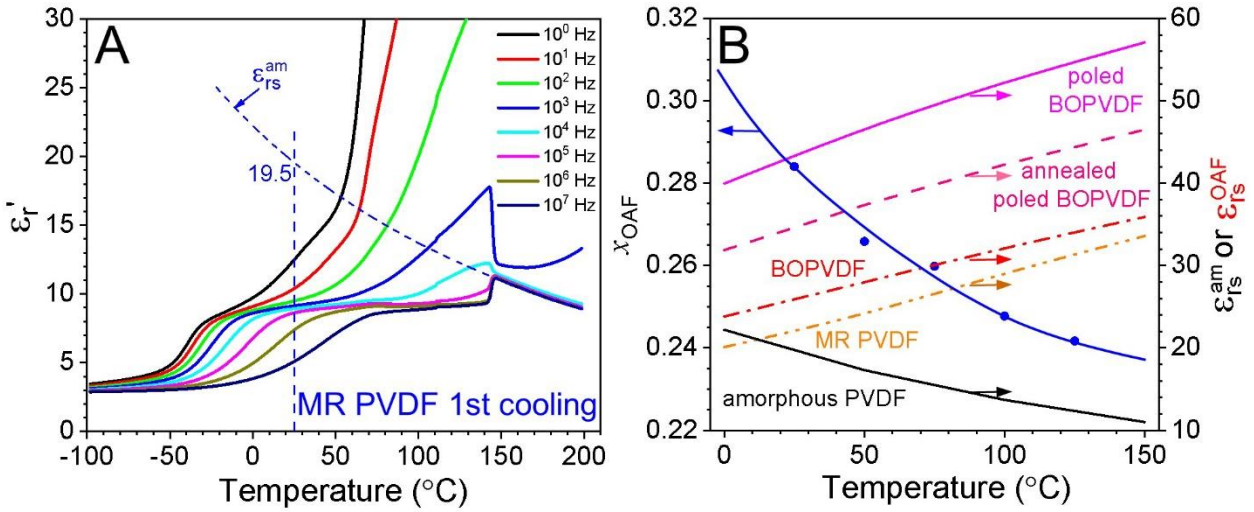

Fig. 9. (A) Temperature-scan ε_r' curves during the first cooling process at 2 °C/min for the MR PVDF under different frequencies. By extrapolation using the Kirkwood-Fröhlich equation (see

Section IV in the Supporting Information), the dielectric constant for the amorphous PVDF (ε_{rs}^{am}) can be obtained at low temperatures. (B) Assuming the x_{OAF} is the same for the fresh BOPVDF, the poled BOPVDF, the 120 °C-annealed poled BOPVDF, and the MR PVDF, the ε_{rs}^{OAF} values are calculated at different temperatures. Meanwhile, the ε_{rs}^{am} is also shown.

Effect of the OAF on the linear dielectric property of PVDF polymers

Once the x_{OAF} is determined, we can use the BDS results in Fig. 3E,G to calculate the static dielectric constants of OAF in the fresh and the highly poled BOPVDF films, respectively, by assuming that they have the same x_c and x_{OAF}. When we consider the three-phase system, the following relationships hold true:

$$\varepsilon_{rs}^{film} - \varepsilon_{r\infty} = x_{OAF}[\varepsilon_{rs}^{OAF} - \varepsilon_{r\infty}] + x_{IAF}[\varepsilon_{rs}^{IAF} - \varepsilon_{r\infty}] \quad (4)$$

$$x_c + x_{OAF} + x_{IAF} = 1 \quad (5)$$

where ε_{rs}^{film}, ε_{rs}^{OAF}, and ε_{rs}^{IAF} are static dielectric constants of the film, the OAF, and the IAF, respectively. $\varepsilon_{r\infty}$ is the dielectric constant of PVDF at high frequencies. It should be nearly the same for different crystals and the amorphous phases, because it originates from electronic and atomic polarizations. In our previous publication, $\varepsilon_{r\infty}$ of PVDF was calculated to be 2.2.[66, 85] The temperature-dependent dielectric constant of the molten or amorphous PVDF (ε_{rs}^{am}) could be determined using the ε_r' of the MR PVDF during cooling, as shown in Fig. 9A (the first cooling and second heating BDS results are shown in Fig. S4). When the frequency was above 10^5 Hz, conduction of impurity ions could be largely ignored before crystallization at 146 °C. It was seen that ε_{rs}^{am} decreased with temperature. This is attributed to the inverse Langevin relationship for the dipolar polarizability of molecular dipoles as a function of temperature.[67] Using the Kirkwood-Fröhlich equation,[67] the ε_{rs}^{am} can be extrapolated to low temperatures (see Fig. S5). For example, ε_{rs}^{am} = 19.5 at 25 °C and 12.1 at 127 °C. In the past, computer simulation was performed to estimate ε_{rs}^{am} of PVDF: 9.7 at 300 K and 12.5 at 400 K.[94] The 400 K result was

similar to what we extrapolated. However, the 300 K result should be incorrect, because it was lower than that at 400 K, which is against the Langevin principle for permanent dipoles.

Assuming the ε_{rs}^{IAF} in the BOPVDF samples was the same as the ε_{rs}^{am}, the ε_{rs}^{OAF} could be calculated using Eqns. (4) and (5). It is interesting to see that the ε_{rs}^{OAF} for both samples increased with temperature, which was against the Langevin principle for mobile permanent dipoles (e.g., the amorphous PVDF in Fig. 9B). It is this increase of ε_{rs}^{OAF} with temperature that kept the overall dielectric constants of different PVDF films almost constant after the α_a relaxation (see Fig. 3A,C,E). This is different from most weakly dipolar polymers, such as polyepichlorohydrin (PECH)[95] and PET,[78] where dielectric constant continuously decreases above the T_g. Currently, it is unclear why the ε_{rs}^{OAF} increases with temperature for these PVDF polymers, whether they contain α or β crystals. Further research should be carried out to understand the underlying mechanism. Meanwhile, the ε_{rs}^{OAF} of the highly poled BOPVDF was significantly higher than that of the fresh BOPVDF. This is attributed to the large P_{r0} in the poled BOPVDF to increase the internal electric field and thus to induce polar nanoregions, like in liquid water.[96] Obviously, it is the high ε_{rs}^{OAF} that makes semicrystalline PVDF a high dielectric constant material at low electric fields (<10 MV/m).

From the ^{1}H ssNMR result in Fig. 1, the x_{OAF} in MR PVDF should be lower than that in the fresh BOPVDF. However, the x_{OAF} value determined from the peak-fitting in the ssNMR spectra was not accurate; therefore, we could not use it. Instead, we could estimate the minimum ε_{rs}^{OAF} of the OAF in the MR PVDF by assuming the upper limit of the x_{OAF} the same as that of the fresh BOPVDF. Meanwhile, a random orientation of the polymer chains was also assumed. As such, those PVDF chains with their axes parallel to the electric field direction would not contribute to the dielectric constant (which accounts for 1/3 of the total contribution). Therefore, we have

the following relationship for the MR PVDF:

$$\varepsilon_{rs}^{film} - \varepsilon_{r\infty} = \frac{2}{3} x_{OAF}[\varepsilon_{rs}^{OAF} - \varepsilon_{r\infty}] + x_{IAF}[\varepsilon_{rs}^{IAF} - \varepsilon_{r\infty}] \quad (6)$$

Fig. 9B also shows the minimum ε_{rs}^{OAF} of the MR PVDF, and it also increased with increasing the temperature. As we can see, it was close to that of the fresh BOPVDF. Considering that the x_{OAF} in the MR PVDF should be somewhat lower than that in the fresh BOPVDF, we infer that the actual ε_{rs}^{OAF} of the MR PVDF should be similar to that of the fresh BOPVDF.

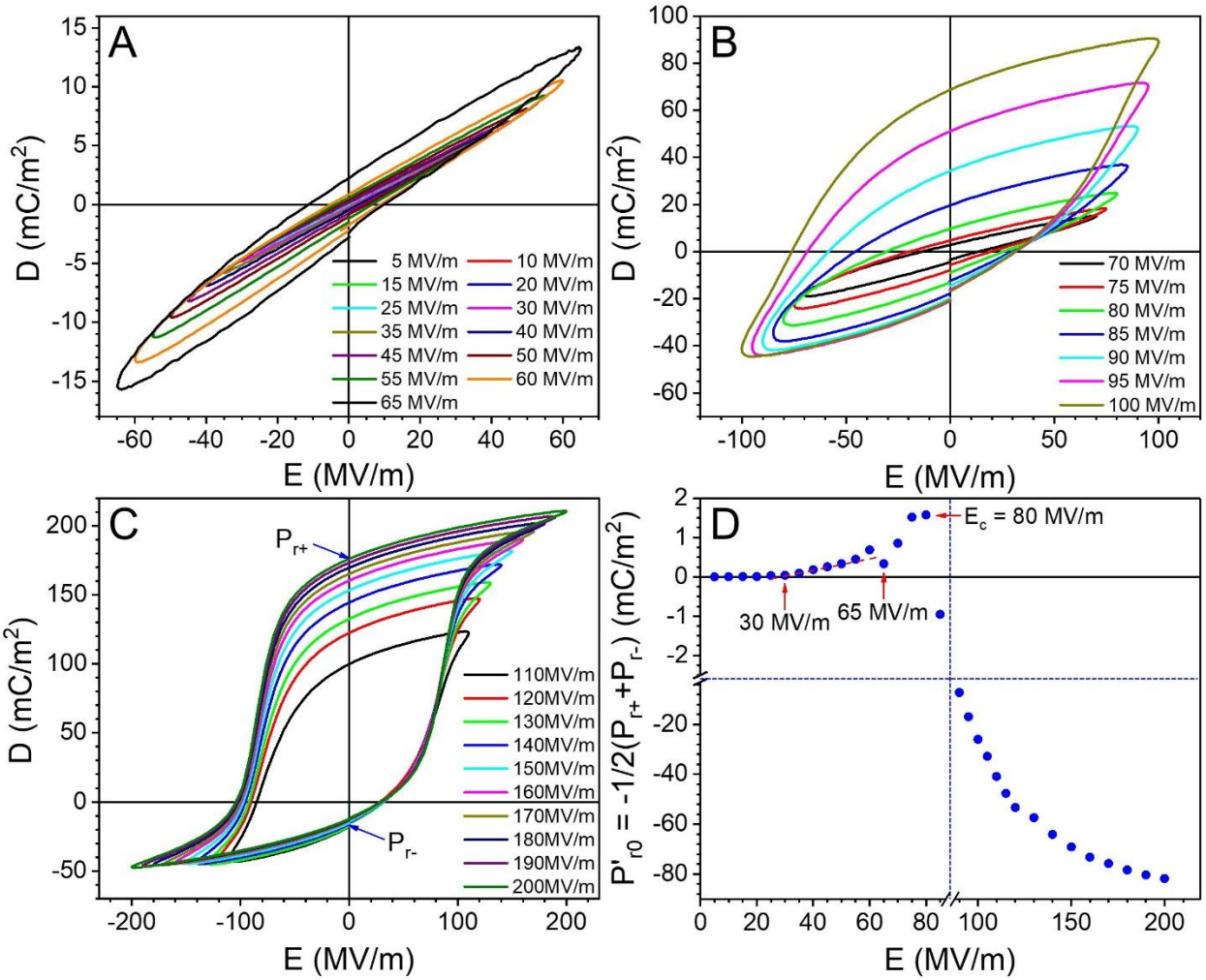

Fig. 10. Bipolar D-E loops for the poled BOPVDF film (with a positive P_{r0}) at room temperature, when the poling field is (A) 5-65 MV/m, (B) 70-100 MV/m, and (C) 110-200 MV/m. (D) The apparent P'_{r0} as a function of the poling electric field at room temperature. The poling electric field has a sinusoidal waveform at 10 Hz, and the second loop is presented here to avoid the

transient effect at the beginning of poling.

Effect of the OAF on the ferroelectric properties of PVDF polymers

For the ferroelectric (i.e., nonlinear dielectric) property, a bipolar D-E loop study was performed on the poled BOPVDF film at room temperature, which had a large positive permanent P_{r0} (i.e., ~118 mC/m^2; see Fig. 7). Fig. 10A-C show the bipolar D-E loops with a gradual increase of the poling field at an increment of 5 MV/m for each step. When the poling field was below 30 MV/m, slim linear loops were observed (Fig. 10A). Between 30 and 60 MV/m, the linear loops became asymmetric with the negative half being broader than the positive half. This is because the positive P_{r0} in the poled BOPVDF caused dielectric nonlinearity. Namely, only when the poling field became negative, certain poor/small-sized positive domains were able to switch to the negative direction. When the poling field increased to 65 MV/m, the positive half loop suddenly became broader. This is because a small portion of the poor domains had already been switched to the negative direction during the previous poling at -60 MV/m. For these poling fields (<65 MV/m), the centers of the bipolar loops were below zero (i.e., D-E loops down-shifted), suggesting a positive P_{r0} detected for the sample. When the poling field increased to 85 MV/m (Fig. 10B), the center of the loop started to shift above zero. This is because a significant amount of ferroelectric domains switched to the negative direction during the previous negative poling at -80 MV/m, leading to a negative P_{r0} in the sample. Further increasing the poling filed to 200 MV/m (Fig. 10C), the centers of the loops kept shifting up.

From this continuous bipolar poling experiment, the bipolar loop could "detect" the apparent remanent polarization (P'_{r0}) implemented by the previous poling loop. The P'_{r0} is defined as:

$$P'_{r0} = -1/2(P_{r+} + P_{r-}) \quad (6)$$

where P_{r+} and P_{r-} are the remanent polarization at the positive and negative sides of the loop, respectively (see Fig. 10C). Fig. 10D shows the P'_{r0} during the continuous bipolar poling process. When the poling field was lower than 30 MV/m, nearly no apparent P'_{r0} was detected. Above 30 MV/m, a small positive P'_{r0} was detected, suggesting that the OAF must start to form ferroelectric domains at this field. When the poling field increased to 65 MV/m, the crystalline ferroelectric domains started to flip to the negative direction at -60 MV/m. Finally, the E_c was seen at 80 MV/m, above which a negative P'_{r0} started to form. Given the fact that the OAF formed switchable ferroelectric domains at a lower electric field (~30 MV/m) than the crystals (60 MV/m), we consider that the ferroelectric switching of the β crystal could be likely induced by the ferroelectric switching of the OAF initiated at the crystal-OAF interfaces. This is the first time that such a fundamental ferroelectric switching mechanism in PVDF is understood.

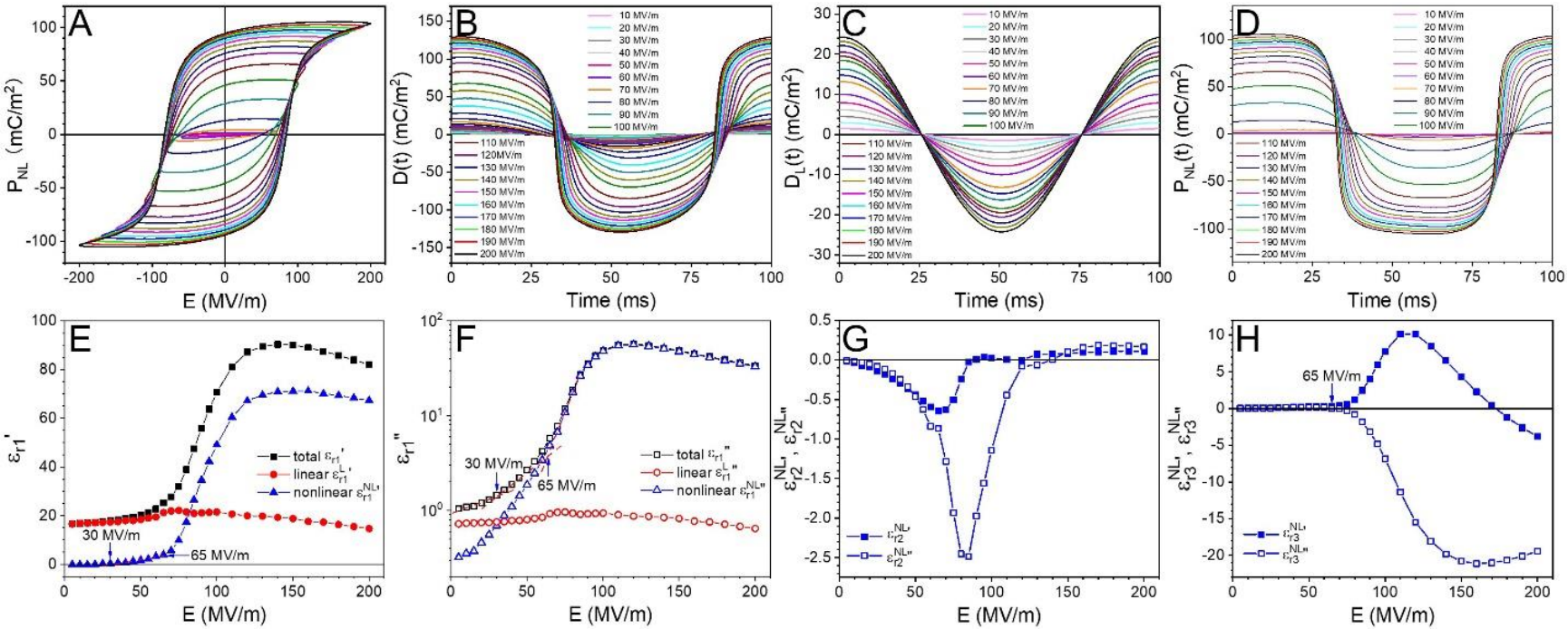

Fig. 11. (A) P_{NL}-E loops for the poled BOPVDF at room temperature after subtraction of D_{def} from the centered bipolar D-E loops in Fig. 10. (B) Total D(t), (C) linear $D_L(t)$, and (D) nonlinear $P_{NL}(t)$ waves for the poled BOPVDF film. After Fourier transform, (E) ε_{r1}', (F) ε_{r1}'', (G) $\varepsilon_{r2}^{NL\prime}/\varepsilon_{r2}^{NL\prime\prime}$, and (H) $\varepsilon_{r3}^{NL\prime}/\varepsilon_{r3}^{NL\prime\prime}$ are obtained for the poled BOPVDF film at room temperature.

The nonlinear dielectric property for the poled BOPVDF film can be quantified from the D-E loop analysis, following previous reports.[87, 97] After subtracting the D_{def}, which is the linear component, the nonlinear P_{NL}-E loops were obtained, as shown in Fig. 11A. From the overall D-E loops (which are centered by subtracting the P'_{r0} from the raw-data loops in Fig. 10), the D_{def}-E loops, and the P_{NL}-E loops, the overall [D(t)], linear [D_L(t)], and nonlinear polarization [P_{NL}(t)] waves were obtained, see Fig. 11B,C,D, respectively. After Fourier transform, the total D_n*, linear (D_1^{L*}), and nonlinear (D_n^{NL*}, n = 1, 2, and 3) polarizations were obtained (see Fig. S6), from which total (ε_{rn}*), linear ($\varepsilon_{r1}^{L\,*}$) and nonlinear dielectric constants (ε_{rn}^{NL*}) were obtained as:

$$\varepsilon_{rn}^{*} = D_n^{*}/\varepsilon_0 E_0 \quad (7)$$

$$\varepsilon_{r1}^{L\,*} = D_1^{L*}/\varepsilon_0 E_0 \quad (8)$$

$$\varepsilon_{rn}^{NL*} = D_n^{NL*}/\varepsilon_0 E_0 \quad (9)$$

where ε_0 is the vacuum permittivity and E_0 is the peak poling field. Fig. 11E,F show both linear and nonlinear components for ε_{r1}' and ε_{r1}'', respectively. First, the linear $\varepsilon_{r1}^{L\,\prime}$ accounted for the total ε_{r1}' below 30 MV/m, above which the nonlinear $\varepsilon_{r1}^{NL\prime}$ started to increase above zero. Similarly, the nonlinear $\varepsilon_{r1}^{NL\prime\prime}$ for the electric field below 30 MV/m was relatively low, i.e., lower than the linear $\varepsilon_{r1}^{L\,\prime\prime}$. Combined with the P'_{r0} result in Fig. 10D, we infer that the ferroelectric switching of the liquid crystal-like OAF should start around 30 MV/m. Second, when the poling field increased to >65 MV/m, the nonlinear $\varepsilon_{r1}^{NL\prime}$ and $\varepsilon_{r1}^{NL\prime\prime}$ drastically increased and the linear $\varepsilon_{r1}^{L\,\prime}$ and $\varepsilon_{r1}^{L\,\prime\prime}$ remained constant or even slightly decreased. Also, the nonlinear $\varepsilon_{r3}^{NL\prime}$ and $\varepsilon_{r3}^{NL\prime\prime}$ started to become significant, indicative of the ferroelectric switching of β crystals in the poled BOPVDF film. Note that even-numbered harmonics should be zero when the sample does not contain any P_{r0}.[87, 97, 98] Because of the large P_{r0} in the poled BOPVDF, finite $\varepsilon_{r2}^{NL\prime}$ and $\varepsilon_{r2}^{NL\prime\prime}$

were observed even below 60 MV/m. Above 60 MV/m, the non-zero $\varepsilon_{r2}^{NL'}$ and $\varepsilon_{r2}^{NL''}$ were resulted from the negative remanent polarization from the previous bipolar poling.

As shown in Fig. 7, the P_{r0} significantly decreased after thermal annealing the poled BOPVDF at >100 °C. To study OAF effect on the ferroelectric property of the pure β BOPVDF with a minimum level of P_{r0}, we annealed the highly poled BOPVDF at 120 °C for 4 days. The P_{r0} decreased to 17 mC/m^2, but did not completely disappear (Fig. S7A). This is consistent with a previous report.[99] The reason that 120 °C was chosen for thermal annealing was to avoid crystal melting, which might induce the crystallization of kinetically favored α crystals after cooling down to room temperature. Indeed, the 120°C-annealed poled BOPVDF sample still kept pure β crystals, as seen in Fig. 2B (the cyan curve). After 120 °C thermal annealing, the ε_{rs}^{a} decreased to 14.8 (Fig. S7B), indicating a reduced ε_{rs}^{OAF} as compared to that in the highly poled BOPVDF (Fig. 9B). Therefore, the poled β crystals in the poled BOPVDF must create a high internal electric field, which enhanced the linear dielectric constant for the OAF. The ferroelectric switching behavior was studied for the 120 °C-annealed poled BOPVDF film by using bipolar D-E loop tests, as shown in Fig. S8. Similar to the result in Fig. 10D, three events were observed at different electric fields (Fig. S8D). The onset of ferroelectric switching of the OAF was seen as early as 25 MV/m, the onset of β crystal ferroelectric switching happened at 55 MV/m, and finally the E_c was observed at 100 MV/m. The nonlinear dielectric property of the 120 °C-annealed poled BOPVDF film was demonstrated in Fig. S9. The above three events were also seen from the nonlinear ε_{r1}*, ε_{r3}*, and ε_{r5}* components.

From both poled and 120 °C-annealed poled BOPVDF samples, the linear dielectric and ferroelectric properties of the OAF become clear. At low fields (<20 MV/m), the OAF has a weak dielectric nonlinearity. Around 25-30 MV/m, the OAF starts to form in-situ ferroelectric

domains imposed by the poling electric field. The ferroelectric switching of the OAF can eventually induce the ferroelectric switching of PVDF β crystals, possibly via the crankshaft-like defects at the OAF-crystal interfaces. However, after removing the poling electric field, the ferroelectric domains in the OAF should largely vanish due to its high thermal motion above the T_g (i.e., the liquid crystal-like nature).

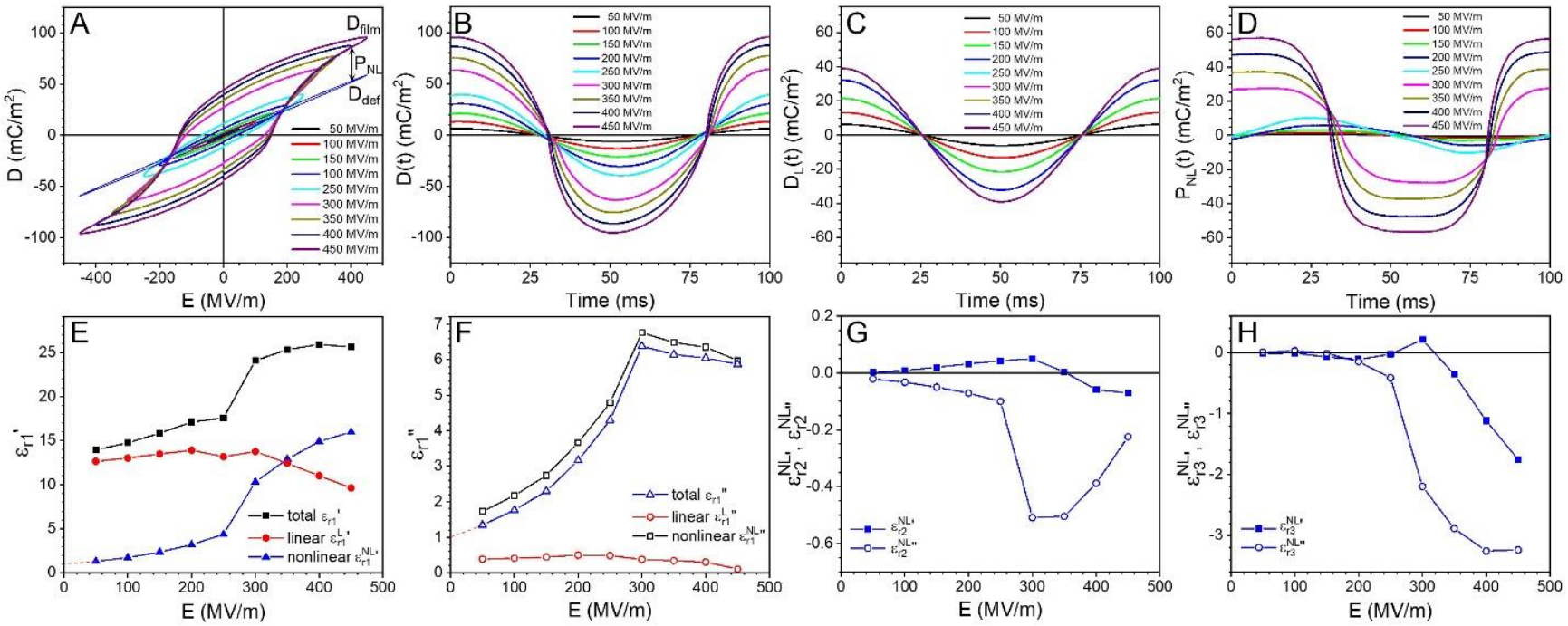

Fig. 12. (A) Bipolar D-E loops for the SC P(VDF-HFP) film at room temperature. The D_{def}-E loops are also shown. After subtracting D_{def} from the total D of the film, the nonlinear P_{NL} is obtained. (B) Total D(t), (C) linear $D_L(t)$, and (D) nonlinear $P_{NL}(t)$ waves for the SC P(VDF-HFP) film. After Fourier transform, (E) ε_{r1}', (F) ε_{r1}'', (G) $\varepsilon_{r2}'/\varepsilon_{r2}''$, and (H) $\varepsilon_{r3}'/\varepsilon_{r3}''$ are obtained for the SC P(VDF-HFP) film.

Effect of the α_c relaxation on the dielectric and ferroelectric properties of PVDF polymers

From the BDS results for the SC P(VDF-HFP) film in Fig. 3A,B, the α_c relaxation could enhance the dielectric constant, but also significantly increase the dielectric loss at the same time. For example, at -20 °C and 1 Hz (i.e., before the α_c relaxation), $\varepsilon_r' = 6.9$ and $\varepsilon_r'' = 0.52$. When the temperature increased to 50 °C at 1 Hz (i.e., after the α_c relaxation), $\varepsilon_r' = 21$ and $\varepsilon_r'' = 2.8$. The dielectric constant increased ~3 times whereas the dielectric loss increased nearly 6 times. Then, we have the following questions: What is the nature of the α_c relaxation? Is it a linear or nonlinear dielectric response of the α PVDF? To answer these questions, we performed a bipolar D-E loop study of the SC P(VDF-HFP) film. The raw D-E loops are shown in Fig. S11, where the apparent P'_{r0} was determined and subtracted before centering the D-E loops (note that the P'_{r0} was rather low below 250 MV/m). The centered second loops under different poling fields are shown in Fig. 12A, together with the linear D_{def}-E loops. Below 250 MV/m, elliptical shaped loops were seen. Above 300 MV/m, typical ferroelectric loops were seen with the E_c around 150 MV/m. After subtracting the D_{def} from the film polarization, the P_{NL}-E loops were obtained (Fig. S11J). Fig. 12B-D show the D_{film}, D_{def}, and P_{NL} waves as a function of time, corresponding to the total, linear, and nonlinear responses of the SC P(VDF-HFP) film. After Fourier transformation, ε_{r1}*, $\varepsilon_{r2}^{NL^*}$, and $\varepsilon_{r3}^{NL^*}$ were obtained from the D_1*, $D_2^{NL^*}$, and $D_3^{NL^*}$ harmonics (see Fig. S12). Results are shown in Fig. 12E-H. The $\varepsilon_{r1}^{L\,\prime}$ kept nearly constant around 13 when the poling field was below 300 MV/m, above which it decreased. Meanwhile, the $\varepsilon_{r1}^{L\,\prime\prime}$ was small. The $\varepsilon_{r1}^{NL\prime}$ gradually increased from 1.3 at 50 MV/m to 4.3 at 250 MV/m, above which a significant increase was observed, indicating a transition to the ferroelectric behavior. This transition was more obvious in the ε_{r1}'', $\varepsilon_{r2}^{NL^*}$, and $\varepsilon_{r3}^{NL^*}$ plots at 300 MV/m (Fig. 12F,G,H). The $\varepsilon_{r2}^{NL^*}$ and $\varepsilon_{r3}^{NL^*}$ values were close to zero below 100 MV/m (Fig. 12G,H).

If we extrapolate both nonlinear ε_{r1}' and ε_{r1}'' to the zero field (Fig. 12E,F), they do not become zero. This indicates that the nonlinearity exists for the α_c relation even at low electric fields. Given the nature of the α_c relaxation, i.e., wagging of several CF_2 dipoles along the polymer chains in the α crystals,[66, 81] we consider that the wagging motions should be cooperative, rather than isolated such as that in a dipolar glass.[100, 101] In this sense, it is similar to the α_a or the glass transition. Namely, a few repeat units along a single α chain must wag at the same time, rather than a single repeat unit wags independently in response to the applied electric field. This cooperative Brownian-like wagging motion should be the nature for the α_c relaxation at low fields. Because no ferroelectric domains are present, the α_c relaxation is paraelectric in nature without any obvious P_r. However, this situation changes when a high electric field (e.g., >250 MV/m) is applied. Many chains in the α crystals start to wag together, forming ferroelectric domains. As a result, an obvious P_r is resulted (see Fig. 12A and Fig. S11J). We conclude that utilizing the α_c relaxation in the α PVDF to enhance the electric energy storage is undesirable, because it has intrinsic dielectric nonlinearity, no matter under low or high electric fields, causing a significant dielectric loss for the material.

Conclusions

Using structural, dielectric, and ferroelectric characterizations, the percentage of the OAF was determined for the fresh and poled BOPVDF films, and MR PVDF. From the BDS study, the RAF quickly devitrified above the T_g around -39 °C, and became mobile OAF around room temperature, which enhanced both dielectric and ferroelectric properties of PVDF. First, the x_{OAF} was determined to be 0.284 at room temperature with $P_{s,OAF} = 0.88P_{s,\beta}$. Second, the ε_{rs}^{OAF} was determined for various PVDF polymers. Surprisingly, it increased with temperature, which is

against the Langevin rule for molecular dipoles. The ε_{rs}^{OAF} increased in the order of MR PVDF, fresh BOVPDF, 120 °C-annealed poled BOPVDF, and poled BOPVDF, suggesting that the crystalline polymorphism (α vs. β) and the macroscopic dipole moment affected the ε_{rs}^{OAF}. Third, the OAF was weakly nonlinear under low fields at temperatures 50 °C above the T_g. At 20-30 MV/m, the poling field started to induce ferroelectric domains for the OAF, which eventually induced ferroelectric switching for the β crystals, possibly via the crankshaft defects at the OAF-crystal interfaces. Finally, the α_c relaxation was found to be intrinsically nonlinear in nature. Below 250 MV/m, the dielectric nonlinearity originated from the cooperative wagging motion along a single α chain. Above 300 MV/m, cooperative CF_2-wagging among many α chains caused the formation of large ferroelectric domains with significant remanent polarization in the sample. The knowledge obtained from this study will help us to further explore new dielectric and ferroelectric properties for other PVDF-based polymers, such as P(VDF-TrFE) copolymers and P(VDF-TrFE-X) terpolymers [X being 1,1-chlorofluoroethylene (CFE) or trichlorofluoroethylene) (CTFE)], which have been introduced in previous reports.[100, 102]

Conflicts of Interest

There are no conflicts to declare.

Acknowledgement

L.Z. acknowledges partial financial support for the SAXS, WAXD, and FTIR measurements from National Science Foundation, Division of Materials Research, Polymers Program (DMR-1708990). T.M. acknowledges partial financial support of the solid-state NMR measurements by NSF DMR Polymers Program (DMR-1708999). This research used the 11-BM

CMS beamline of National Synchrotron Light Source-II (NSLS-II), Brookhaven National Laboratory (BNL), a U.S. Department of Energy User Facility operated for the Office of Science by BNL under Contract DE-SC0012704. L.Z. also acknowledges helpful discussion with Prof. Jerry Bernholc at North Carolina State University.

References

1. H. S. Nalwa, ed., *Ferroelectric Polymers: Chemistry, Physics, and Applications*, Marcel Dekker, New York, 1995.
2. T. Correia and Q. Zhang, eds., *Electrocaloric Materials: New Generation of Coolers*, Springer, New York, 2013.
3. R. G. Kepler, Ferroelectric, pyroelectric, and piezoelectric properties of poly(vinylidene fluoride), in *Ferroelectric Polymers: Chemistry, Physics, and Applications*, H. S. Nalwa, ed., Marcel Dekker, Inc., New York, 1995, Chapter 3, pp.183-232.
4. H. Ohigashi and T. Hattori, *Jpn. J. Appl. Phys.*, 1989, **28,** L1612-L1615.
5. Y. Takase, H. Tanaka, T. T. Wang, R. E. Cais and J. M. Kometani, *Macromolecules*, 1987, **20,** 2318-2320.
6. F. Bauer, *Ferroelectrics*, 1983, **49,** 231-240.
7. K. Nakamura, M. Nagai, T. Kanamoto, Y. Takahashi and T. Furukawa, *J. Polym. Sci., Part B: Polym. Phys.*, 2001, **39,** 1371-1380.
8. K. Tashiro, M. Kobayashi, H. Tadokoro and E. Fukada, *Macromolecules*, 1980, **13,** 691-698.
9. C. K. Purvis and P. L. Taylor, *Phys. Rev. B*, 1982, **26,** 4547-4563.
10. C. K. Purvis and P. L. Taylor, *J. Appl. Phys.*, 1983, **54,** 1021-1028.
11. R. Al-Jishi and P. L. Taylor, *J. Appl. Phys.*, 1985, **57,** 902-905.

12. J. D. Carbeck, D. J. Lacks and G. C. Rutledge, *J. Chem. Phys.*, 1995, **103,** 10347-10355.

13. J. D. Carbeck and G. C. Rutledge, *Polymer*, 1996, **37,** 5089-5097.

14. S. M. Nakhmanson, M. B. Nardelli and J. Bernholc, *Phys. Rev. Lett.*, 2004, **92,** 115504.

15. S. M. Nakhmanson, M. B. Nardelli and J. Bernholc, *Phys. Rev. B*, 2005, **72,** 115210.

16. A. Itoh, Y. Takahashi, T. Furukawa and H. Yajima, *Polym. J.*, 2014, **46,** 207-211.

17. B. Wunderlich, *Macromolecular Physics, vol. 1: Crystal Structure, Morphology, and Defects*, Academic Press, New York, 1973.

18. B. Lotz, T. Miyoshi and S. Z. D. Cheng, *Macromolecules*, 2017, **50,** 5995-6025.

19. L. Mandelkern, *Acc. Chem. Res.*, 1990, **23,** 380-386.

20. B. Wunderlich, *Prog. Polym. Sci.*, 2003, **28,** 383-450.

21. W. Chen and B. Wunderlich, *Macromol. Chem. Phys.*, 1999, **200,** 283-311.

22. H. Janeschitz-Kriegl, *Crystallization Modalities in Polymer Melt Processing : Fundamental Aspects of Structure Formation*, Springer, New York, 2010.

23. M. T. DeMeuse, *Biaxial Stretching of Film Principles and Applications*,Woodhead Pub., Oxford, U.K., 2011.

24. T. Nakajima, K. Kajiwara and J. E. McIntyre, *Advanced Fiber Spinning Technology*, Woodhead Pub., Cambridge, U.K., 1994.

25. A. Esposito, N. Delpouve, V. Causin, A. Dhotel, L. Delbreilh and E. Dargent, *Macromolecules*, 2016, **49,** 4850-4861.

26. H. Chen and P. Cebe, *Macromolecules*, 2009, **42,** 288-292.

27. M. C. Righetti, M. Laus and M. L. Di Lorenzo, *Eur. Polym. J.*, 2014, **58,** 60-68.

28. R. Androsch and B. Wunderlich, *Polymer*, 2005, **46,** 12556-12566.

29. M. L. Di Lorenzo, M. C. Righetti, M. Cocca and B. Wunderlich, *Macromolecules*, 2010, **43,**

7689-7694.

30. Q. Ma, G. Georgiev and P. Cebe, *Polymer*, 2011, **52,** 4562-4570.
31. S. Z. D. Cheng and B. Wunderlich, *Macromolecules*, 1988, **21,** 789-797.
32. G. Schoukens, *Polymer*, 1999, **40,** 5637-5645.
33. D. F. Miranda, S. Zhang and J. Runt, *Macromolecules*, 2017, **50,** 8083-8096.
34. S. Z. D. Cheng, M. Y. Cao and B. Wunderlich, *Macromolecules*, 1986, **19,** 1868-1876.
35. P. Huo and P. Cebe, *Macromolecules*, 1992, **25,** 902-909.
36. H. Xu and P. Cebe, *Macromolecules*, 2004, **37,** 2797-2806.
37. S. Z. D. Cheng, Z. Q. Wu and B. Wunderlich, *Macromolecules*, 1987, **20,** 2802-2810.
38. P. Huo and P. Cebe, *J. Polym. Sci., Part B: Polym. Phys.*, 1992, **30,** 239-250.
39. S. X. Lu and P. Cebe, *Polymer*, 1996, **37,** 4857-4863.
40. C. Schick, A. Wurm and A. Mohamed, *Colloid Polym. Sci.*, 2001, **279,** 800-806.
41. H. Chen and P. Cebe, *J. Therm. Anal. Calorim.*, 2007, **89,** 417-425.
42. I. Kolesov and R. Androsch, *Polymer*, 2012, **53,** 4770-4777.
43. E. Zuza, J. M. Ugartemendia, A. Lopez, E. Meaurio, A. Lejardi and J. R. Sarasua, *Polymer*, 2008, **49,** 4427-4432.
44. M. C. Righetti and E. Tombari, *Thermochim. Acta*, 2011, **522,** 118-127.
45. M. L. Di Lorenzo, M. Gazzano and M. C. Righetti, *Macromolecules*, 2012, **45,** 5684-5691.
46. A. Wurm, E. Zhuravlev, K. Eckstein, D. Jehnichen, D. Pospiech, R. Androsch, B. Wunderlich and C. Schick, *Macromolecules*, 2012, **45,** 3816-3828.
47. R. Androsch, M. L. Di Lorenzo, C. Schick and B. Wunderlich, *Polymer*, 2010, **51,** 4639-4662.
48. J. Grebowicz, S. F. Lau and B. Wunderlich, *J. Polym. Sci.: Polym. Symp.*, 1984, **71,** 19-37.

49. Q. Zia, D. Mileva and R. Androsch, *Macromolecules*, 2008, **41,** 8095-8102.

50. M. L. Di Lorenzo, M. C. Righetti and B. Wunderlich, *Macromolecules*, 2009, **42,** 9312-9320.

51. R. Kitamaru, F. Horii and K. Murayama, *Macromolecules*, 1986, **19,** 636-643.

52. I. S. Kolesov, R. Androsch and H. J. Radusch, *Macromolecules*, 2005, **38,** 445-453.

53. S. Z. D. Cheng, R. Pan and B. Wunderlich, *Makromol. Chem.*, 1988, **189,** 2443-2458.

54. M. Pyda, E. Nowak-Pyda, J. Mays and B. Wunderlich, *J. Polym. Sci., Part B: Polym. Phys.*, 2004, **42,** 4401-4411.

55. G. Dlubek, A. Sen Gupta, J. Pionteck, R. Häßler,, R. Krause-Rehberg, H. Kaspar and K. H. Lochhaas, *Polymer*, 2005, **46,** 6075-6089.

56. G. Calleja, A. Jourdan, B. Ameduri and J. P. Habas, *Eur. Polym. J.*, 2013, **49,** 2214-2222.

57. S. Z. D. Cheng and B. Wunderlich, *Macromolecules*, 1987, **20,** 1630-1637.

58. J. Pak, M. Pyda and B. Wunderlich, *Macromolecules*, 2003, **36,** 495-499.

59. K. Ishikiriyama, M. Pyda, G. Zhang, T. Forschner, J. Grebowicz and B. Wunderlich, *J. Macromol. Sci., Part B: Phys*, 1998, **B37,** 27-44.

60. M. Pyda, M. L. Di Lorenzo, J. Pak, P. Kamasa, A. Buzin, J. Grebowicz and B. Wunderlich, *J. Polym. Sci., Part B: Polym. Phys.*, 2001, **39,** 1565-1577.

61. B. Hahn, J. Wendorff and D. Y. Yoon, *Macromolecules*, 1985, **18,** 718-721.

62. B. R. Hahn, O. Herrmann-schönherr, and J. H. Wendorff, *Polymer*, 1987, **28,** 201-208.

63. T. Ando, T. Hanada and K. Saitoh, *J. Polym. Sci., Part B: Polym. Phys.*, 1994, **32,** 179-185.

64. J. Mijovic, J. Sy and T. K. Kwei, *Macromolecules*, 1997, **30,** 3042-3050.

65. B. Lu, K. Lamnawar, A. Maazouz and H. Zhang, *Soft Matter*, 2016, **12,** 3252-3264.

66. L. Yang, J. Ho, E. Allahyarov, R. Mu and L. Zhu, *ACS Appl. Mater. Interfaces*, 2015, **7,** 19894-19905.

67. K. C. Kao, *Dielectric Phenomena in Solids: with Emphasis on Physical Concepts of Electronic Processes*, Elsevier Academic Press, Boston, 2004.

68. A. Gradys, P. Sajkiewicz, S. Adamovsky, A. Minakov and C. Schick, *Thermochim. Acta*, 2007, **461,** 153-157.

69. N. D. Govinna, Ph.D. Dissertation, Tufts University, 2019.

70. A. Gradys, P. Sajkiewicz, E. Zhuravlev and C. Schick, *Polymer*, 2016, **82,** 40-48.

71. V. Sencadas, R. Gregorio and S. Lanceros-Mendez, *J. Macromol. Sci. B*, 2009, **48**, 514-525.

72. H. L. Guo, Y. Zhang, F. F. Xue, Z. W. Cai, Y. R. Shang, J. Q. Li, Y. Chen, Z. H. Wu and S. C. Jiang, *CrystEngComm*, 2013, **15**, 1597-1606.

73. L. Li, M. Q. Zhang, M. Z. Rong and W. H. Ruan, *RSC Adv.*, 2014, **4**, 3938-3943.

74. T. R. Jow and P. J. Cygan, *J. Appl. Phys.*, 1993, **73,** 5147-5151.

75. F. X. Guan, J. L. Pan, J. Wang, Q. Wang and L. Zhu, *Macromolecules*, 2010, **43,** 384-392.

76. C. Hedesiu, D. E. Demco, R. Kleppinger, G. Vanden Poel, W. Gijsbers, B. Blumich, K. Remerie and V. M. Litvinov, *Macromolecules*, 2007, **40,** 3977-3989.

77. W. Gabrielse, H. A. Gaur, F. C. Feyen and W. S. Veeman, *Macromolecules*, 1994, **27,** 5811-5820.

78. Y. Li, Y. Makita, G. Zhang, G. Rui, Z.-M. Li, G.-J. Zhong, T. Miyoshi, H.-D. Huang and L. Zhu, *Macromolecules*, 2020, **53,** 3967-3977.

79. K. Nakagawa and Y. Ishida, *J. Polym. Sci., Part B: Polym. Phys.*, 1973, **11,** 2153-2171.

80. H. Sasabe, S. Saito, M. Asahina and H. Kakutani, *J. Polym. Sci., A-2, Polym. Phys.*, 1969, **7,** 1405-1414..

81. M. A. Bachmann and J. B. Lando, *Macromolecules*, 1981, **14,** 40-46.

82. X. Chen, E. Allahyarov, Q. Li, D. Langhe, M. Ponting, D. E. Schuele, E. Baer and L. Zhu,

Compos. B Eng., 2020, **190,** 107908.

83. M. A. Marcus, *IEEE Trans. Electr. Insul.*, 1986, **EI-21,** 519-523.
84. R. Jr. Gregorio and E. M. Ueno, *J. Mater. Sci.*, 1999, **34,** 4489-4500.
85. N. Karasawa and W. A. Goddard III, *Macromolecules*, 1992, **25,** 7268-7281.
86. H. Ohigashi, *J. Appl. Phys.*, 1976, **47,** 949-955.
87. Y. Li, J. Ho, J. Wang, Z.-M. Li, G.-J. Zhong and L. Zhu, *ACS Appl. Mater. Interfaces*, 2016, **8,** 455-465.
88. M. Womes, E. Bihler and W. Einsenmenger, *IEEE Trans. Dielectr. Electr. Insul.*, 1989, **24,** 461-468.
89. C. A. Avila-Orta, F. J. Medellin-Rodriguez, Z.-G. Wang, D. Navarro-Rodriguez, B. S. Hsiao and F. J. Yeh, *Polymer*, 2003, **44,** 1527-1535.
90. M. G. Broadhurst and G. T. Davis, *Ferroelectrics*, 1984, **60,** 3-13.
91. I. Katsouras, K. Asadi, M. Li, T. B. van Driel, K. S. Kjaer, D. Zhao, T. Lenz, Y. Gu, P. M. Blom, D. Damjanovic, M. M. Nielsen and D. M. de Leeuw, *Nat. Mater.*, 2016, **15,** 78-84.
92. S. M. Feng, Y. S. Chai, J. L. Zhu, N. Manivannan, Y. S. Oh, L. J. Wang, Y. S. Yang, C. Q. Jin and K. H. Kim, *New J. Phys.*, 2010, **12,** 073006.
93. J. Jones, L. Zhu, N. Tolk and R. Mu, *Appl. Phys. Lett.*, 2013, **103,** 072901.
94. N. Karasawa and W. A. Goddard, *Macromolecules*, 1995, **28,** 6765-6772.
95. Y.-F. Zhu, Z. Zhang, M. H. Litt and L. Zhu, *Macromolecules*, 2018, **51,** 6257-6266.
96. D. C. Elton and M. V. Fernandez-Serra, *J. Chem. Phys.*, 2014, **140,** 124504.
97. C. H. Tsang and F. G. Shin, *J. Appl. Phys.*, 2003, **93,** 2861-2865.
98. T. Furukawa, K. Nakajima, T. Koizumi and M. Date, *Jpn. J. Appl. Phys.*, 1987, **26,** 1039-1045.

99. M. P. Silva, C. M. Costa, V. Sencadas, A. J. Paleo and S. Lanceros-Mendez, *J. Polym. Res.*, 2011, **18,** 1451-1457.

100. L. Zhu, *J. Phys. Chem. Lett.*, 2014, **5,** 3677-3687.

101. J. Wei and L. Zhu, *Prog. Polym. Sci.*, 2020, **106,** 101254.

102. L. Yang, X. Li, E. Allahyarov, P. L. Taylor, Q. M. Zhang and L. Zhu, *Polymer*, 2013, **54,** 1709-1728.

TOC Graphic

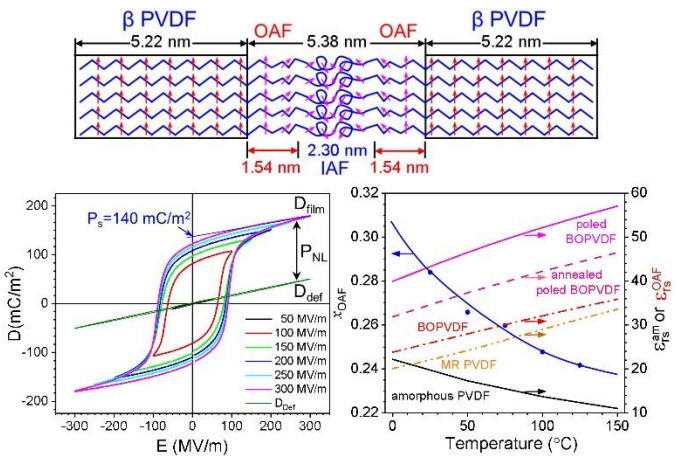

Highlight

Oriented amorphous fraction in biaxially oriented poly(vinylidene fluoride) renders it significantly enhanced dielectric and ferroelectric properties.